1993ApJ...403..690B

THE ASTROPHYSICAL JOURNAL, 403:690–705, 1993 February 1
© 1993. The American Astronomical Society. All rights reserved. Printed in U.S.A.

CAN WE OBSERVE ACCRETING, ISOLATED NEUTRON STARS?

OMER BLAES
Canadian Institute for Theoretical Astrophysics, University of Toronto, 60 St. George Street, Toronto, ON, Canada M5S 1A1
AND
PIERO MADAU
Department of Physics and Astronomy, The Johns Hopkins University; and Space Telescope Science Institute, 3700 San Martin Drive, Baltimore MD 21218[1]
Received 1992 June 2; accepted 1992 August 3

ABSTRACT

We discuss the observability of isolated neutron stars (NSs) accreting interstellar material as sources of quiescent and transient UV and X-ray radiation. We study their spatial and kinematic properties in the solar neighborhood through Monte Carlo simulations of 10^5 orbits in the Galactic potential. We present a much faster semianalytic technique which is capable of reproducing the *full* kinematic properties of the local NS population, in remarkable agreement with the Monte Carlo results. We derive the accretion rate distributions associated with the various phases of the interstellar medium (ISM). Assuming blackbody emission and 10^9 NSs in the Galaxy, we estimate that, in the case of isotropic (polar cap) accretion, $\sim$2000 (10,000) old NSs should be observed as X-ray sources in the *ROSAT* XRT all-sky survey, with up to 600 (100) of them showing up at longer wavelengths in the *ROSAT* WFC survey. The number of detectable NSs in the forthcoming *EUVE* all-sky survey should be close to 200 (20). If old NSs are magnetized, we estimate that an additional 1000 sources located in giant molecular clouds should be observed in the *ROSAT* XRT survey. NSs detected by *ROSAT* XRT will be strongly concentrated toward the Galactic plane. Isolated NSs in the local cavity can contribute only 0.1% of the soft X-ray background at 100 eV. We argue, however, that the integrated emission from solitary NSs accreting material in the Galactic plane could give rise to the Galactic X-ray ridges observed by *EXOSAT* and *HEAO 1* A-2. We investigate the emission properties of accreting NSs moving supersonically in dense atomic and molecular clouds, and show that they will produce elongated, "cometary" H II regions, a possible characteristic observational signature. Material accumulated by slow accretion onto the polar cap of magnetized NSs located in diffuse clouds might be unstable to nuclear burning and lead to X-ray bursts. We estimate a rate of 25 yr^{-1} energetic, $\sim 5 \times 10^{37}$ ergs events within 1 kpc, which might be detectable by *HETE*. Such bursts may also be responsible for some of the fast X-ray transients observed by *HEAO 1* A-1. We emphasize the sensitive dependence of these estimates on the uncertain kinematic properties of radio pulsars, total number of NSs produced throughout the history of the Galaxy, geography of the local ISM, magnetic field topology and evolution, physics of the accretion process, and emission properties.

Subject headings: accretion, accretion disks — stars: neutron — stars: statistics — X-rays: bursts — X-rays: stars

1. INTRODUCTION

Neutron stars are believed to be the powerhouses of many astrophysical phenomena, notably pulsars, X-ray binaries and bursters, and possibly gamma-ray bursts. In this paper we discuss the exciting possibility of observing that large population of old, isolated NSs which, no longer active as pulsars, are currently accreting material from the interstellar medium.

The possibility that such a population might be observable because of the liberation of gravitational energy from infalling interstellar material was first studied by Ostriker, Rees, & Silk (1970). They predicted an enhancement of Galactic diffuse emission in soft X-rays, and noted that the nearest NS might be detectable as a thermal X-ray source. (The X-ray emission properties of isolated NSs have been reviewed by Helfand, Chanan, & Novick 1980.) Treves & Colpi (1991, hereafter TC) have recently reconsidered the question. They discussed magnetized NSs accreting from a uniform interstellar medium (ISM) and derived the X-ray luminosity function by adopting a speed distribution based on Monte Carlo calculations by Paczyński (1990). TC estimated that $\sim$5000 sources, a large fraction of the total NS population within 140 pc, could be detected by the *ROSAT* all-sky survey. The potential importance of such observations cannot be overstated: they would represent a unique diagnostic tool of NS properties, such as number densities and star formation histories; masses, radii, and magnetic fields; and the physics of the accretion process.

In this paper we greatly expand and extend these analyses of the statistics and potentially observable properties of the accreting NS population in the solar neighborhood. The simple models adopted here make definite predictions of hitherto unobserved phenomena, by which our understanding of the physical processes at work might be tested. We limit our discussion to quiescent and transient phenomena which do not require knowledge of the total accretion history of the star, such as those associated with the slow buildup of accreted material over the lifetime of the Galaxy (Blaes et al. 1990, 1992). A correct assessment of the distribution of interstellar accretion rates onto isolated NSs requires knowledge of the *present* spatial and speed distributions relative to the interstellar material, which we discuss in § 2. An accurate description of the morphology and physical state of the local ISM is

[1] Postal address.

© American Astronomical Society • Provided by the NASA Astrophysics Data System

1993ApJ...403..690B

also needed: these are reviewed in § 3. In § 4 we reconsider the problem of interstellar accretion onto old NSs, and provide numbers and accretion rate distributions for each of the various local phases. The detectability of isolated NSs in the solar neighborhood by the *ROSAT* (completed) and *Extreme Ultraviolet Explorer* (*EUVE*) (forthcoming) surveys is discussed in § 5. We show that aging NSs represent a substantial population of low-luminosity Galactic UV and soft X-ray sources. We suggest that unresolved accreting NSs may contribute the bulk of the integrated X-ray emission from the Galactic plane. In § 6 we examine the emission properties of NSs accreting material in dense atomic and molecular clouds. Finally, we summarize our conclusions in § 7.

2. SPATIAL AND KINEMATIC PROPERTIES OF OLD NEUTRON STARS

Using Monte Carlo simulations of orbits, a number of workers have investigated the distribution of old NSs in the Galaxy (Paczyński 1990; Hartmann, Epstein, & Woosley 1990; Blaes & Rajagopal 1991, hereafter BR91). These authors have made a variety of assumptions concerning the Galactic gravitational potential, the NS birthrate, and the NS birth distribution. The gravitational potential is determined observationally, although with some uncertainties. The birth properties of NSs are inferred by assuming they are identical to those of young radio pulsars which are observed today. These properties are not well known, and both the birth distribution and the birthrate could have varied in the past. Moreover, there may exist isolated NSs which do not pass through a radio pulsar phase, and whose birth properties could therefore be very different. Monte Carlo simulations are too time-consuming to make it feasible to explore all the plausible possibilities.

Much faster semianalytic techniques of calculating the kinematic properties of old NSs have also been devised. Frei, Huang, & Paczyński (1992, hereafter FHP) have presented a method of calculating the vertical density and velocity distributions of Galactic disk NSs, within the assumption that the gravitational potential may be approximated as a function only of the height z above the Galactic plane. They were able to reproduce the Monte Carlo simulation results accurately. However, the radial and azimuthal velocity distributions are also necessary to calculate accretion rates. BR91 presented a technique for obtaining the full three-dimensional velocity distribution valid within the epicyclic approximation, but they also realized that, if all NSs share the birth properties of the present-day radio pulsar population, the majority of Galactic disk NSs will be moving too fast relative to the ISM for this approximation to be valid. In this section we generalize the method of FHP to obtain a semianalytic technique capable of reproducing the full kinematic properties of the local NS population. We compare the results of this technique with that of a Monte Carlo simulation and find that they are in remarkable agreement.

2.1. *The Monte Carlo Simulation*

The simulation is similar to that presented in BR91. The Galactic potential Φ is made up of three parts. The disk and spheroid components are given by

$$\Phi_j(R, z) = \frac{-GM_j}{\{R^2 + [a_j + (z^2 + b_j^2)^{1/2}]^2\}^{1/2}}, \quad (1)$$

where R is the projected radial distance from the Galactic center in the Galactic plane, and $j = s, d$ stands for the spheroid or disk component, respectively. The halo component is given by

$$\Phi_h(r) = \frac{GM_h}{r_h}\left[\frac{1}{2}\ln\left(1 + \frac{r^2}{r_h^2}\right) + \frac{r_h}{r}\tan^{-1}\left(\frac{r}{r_h}\right)\right], \quad (2)$$

where $r \equiv (R^2 + z^2)^{1/2}$ is the distance from the Galactic center. The numerical values of the parameters in the potential are $a_s = 0$, $b_s = 0.277$ kpc, $M_s = 1.12 \times 10^{10}\ M_\odot$, $a_d = 4.20$ kpc, $b_d = 0.198$ kpc, $M_d = 8.78 \times 10^{10}\ M_\odot$, $r_h = 6.0$ kpc, and $M_h = 5.0 \times 10^{10}\ M_\odot$. The solar Galactocentric radius R_0 is at 8.5 kpc; the local circular speed, volume density, and surface density (within ± 700 pc) are $v_g(R_0) = 220$ km s^{-1}, 0.18 $M_\odot$ pc^{-3}, and 75 $M_\odot$ pc^{-2}, respectively (BR91).

The assumed *initial* distribution of each velocity component $(v_{Ri}, v_{\phi i}, v_{zi})$, relative to the local circular speed, is Gaussian:

$$p(v_{Ri}, v_{\phi i}, v_{zi}) = \frac{1}{(2\pi)^{3/2}\sigma_v^3}\exp\left(-\frac{v_i^2}{2\sigma_v^2}\right), \quad (3)$$

where $v_i^2 = v_{Ri}^2 + [v_{\phi i} - v_g(R_i)]^2 + v_{zi}^2$. The probability density that a NS is born at height z_i above the Galactic plane is also Gaussian:

$$p(z_i) = \frac{1}{(2\pi)^{1/2}\sigma_z}\exp\left(-\frac{z_i^2}{2\sigma_z^2}\right). \quad (4)$$

These distributions were used by Narayan & Ostriker (1990, hereafter NO) to fit the radio pulsar statistics, except that in their case σ_v also depended on the initial pulsar magnetic field strength B_i. Hence the true initial velocity distribution is calculated by integrating equation (3) over the distribution of B_i. In their most likely "model b," NO also had two separate ("F" and "S") pulsar populations with different birth distribution parameters. Because we are only interested in testing our approximations using the Monte Carlo simulation, we consider for the moment only F population pulsars born with initial magnetic field at the peak of the NO distribution ($\log_{10} B_i = 12.61$). This then gives $\sigma_v = 60.76$ km s^{-1} and $\sigma_z = 150$ pc.[2]

We adopt a radial birth distribution which is similar to that of the stellar disk, an exponential with scale length 4.5 kpc out to a maximum radius $R_{\max} = 20$ kpc, i.e.,

$$p(R_i) = a_R\frac{R_i}{R_d^2}\exp\left(-\frac{R_i}{R_d}\right), \quad (5)$$

where $R_d = 4.5$ kpc and

$$a_R = [1 - e^{-R_{\max}/R_d}(1 + R_{\max}/R_d)]^{-1}.$$

BR91 integrated 2×10^4 orbits for 10^{10} yr, the assumed lifetime of the Galaxy. They found that the local number density of stars, averaged over the region 7.5 kpc $< R <$ 9.5 kpc and $|z| < 40$ pc, is $n_{\rm NS}^{\rm F} \simeq 1.1 \times 10^{-12} N_{\rm tot}^{\rm F}$ pc^{-3}, where $N_{\rm tot}^{\rm F}$ is the total number of F NSs born in the Galaxy from the above birth distributions. The representative kinematic properties of this stellar distribution averaged over the region 7.5 kpc $< R <$ 9.5 kpc and over all heights are $\langle v_R^2\rangle^{1/2} \simeq 66$

[2] Note that this is also the prescription which was used to simulate the F population stars in BR91. From the results of § 2.3 below, this neglect of the initial magnetic field distribution is unlikely to have greatly affected their results.

© American Astronomical Society • Provided by the NASA Astrophysics Data System

1993ApJ...403..690B

km s^{-1}, $\langle[v_\phi - v_g(R_0)]^2\rangle^{1/2} \simeq 51$ km s^{-1}, $\langle v_z^2\rangle^{1/2} \simeq 38$ km s^{-1}, and $\langle v_\phi - v_g(R_0)\rangle \simeq -22$ km s^{-1}.

The number of NSs falls off with the height z above the Galactic plane, with $\langle z^2\rangle^{1/2} \simeq 650$ pc. The height at which the NS density falls to half the midplane value is $z_{1/2} \simeq 300$ pc. The steady state z-distribution is clearly far from Gaussian. This may affect some of the results of NO, since their analysis assumed a time-evolving z-distribution which is always Gaussian.

To improve the statistics in the low and high-velocity bins, we have calculated 10^5 orbits (5 times the number of orbits calculated in BR91) which were energetically capable of passing within the cylindrical shell described by 7.5 kpc $< R <$ 9.5 kpc. During their passage through this "solar region," their three-dimensional speed relative to the local circular speed for various ranges of heights above the Galactic plane was stored every 10^6 yr over a total orbital time of 10^{10} yr. We have computed in this way the distribution function of stars born at a uniform rate throughout the history of the Galaxy, each binning at time t representing a NS currently present at that point in phase space but born a time t ago. One orbit integration therefore samples the behavior of 10^4 stars born at different times with the same initial conditions. Using this method (Paczyński 1990), we were able to generate 10^9 stellar positions overall, with approximately 25% of them in the solar region. Over the lifetime of the Galaxy the stars will phase-mix. The final phase-space distribution will be in equilibrium and therefore independent of the assumption of a uniform birthrate.

The differential NS speed distribution is shown in Figure 1, averaged over the region 7.5 kpc $< R <$ 9.5 kpc and various height ranges. For stars with $|z| < 200$ pc we find $\langle v\rangle \simeq 79$ km s^{-1} and $\langle v^2\rangle^{1/2} \simeq 87$ km s^{-1}.

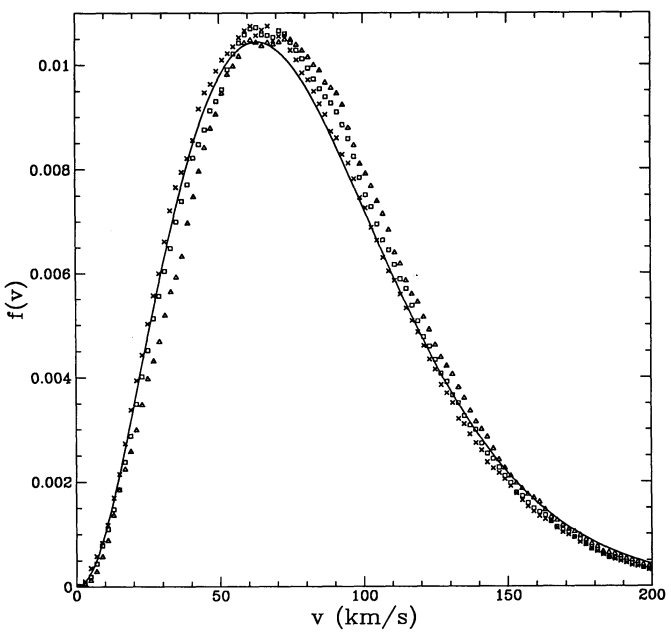

FIG. 1.—Speed distribution in the solar neighborhood for the (single initial magnetic field) F population. Points are from the Monte Carlo simulation for the region 7.5 kpc $< R <$ 9.5 kpc with $|z| < 200$ pc (*crosses*), 200 pc $< |z| <$ 400 pc (*squares*), and 400 pc $< |z| <$ 600 pc (*triangles*). The curve is the thin-disk approximation to the speed distributions at $R = R_0 = 8.5$ kpc and $z = 200$ pc. The data are normalized to unit area.

2.2. *The Thin-Disk Approximation*

According to the strong Jeans theorem, the equilibrium NS distribution function depends only on the three isolating integrals of motion in the Galactic gravitational potential. Two of these integrals are the specific angular momentum, $L_z = Rv_\phi$, and the total energy E. Unfortunately, the third integral is not known. If it were, then the equilibrium distribution function could be obtained directly from the distribution of these three integrals in the birth distribution function.

The results of the Monte Carlo simulation suggest that the local NS population will be dominated by stars whose orbits do not carry them far out of the Galactic plane. Near the plane, the vertical dependence of the potential is much steeper than the radial dependence, implying that most stars which pass through the solar region will have $E_z \equiv v_z^2/2 + \Phi(R_0, z)$ as an approximate integral of motion. As shown by FHP, this is an excellent approximation for reproducing the vertical equilibrium spatial and velocity distributions. If this is true, however, then $E - E_z = v_R^2/2 + v_\phi^2/2 + \Phi(R, z) - \Phi(R_0, z)$ must also be an approximate integral of motion. Moreover, the vertical oscillation frequency for disk stars is much larger than the radial oscillation frequency. This suggests that we average over the vertical motions and treat $E_R \equiv v_R^2/2 + v_\phi^2/2 + \Phi(R, 0)$ as an approximate integral of motion.

In the following, we will denote this set of assumptions as the "thin-disk approximation." Within this limit, the vertical motions of NSs are controlled by the potential $\Phi(R_0, z)$, while radial motions are controlled by $\Phi(R, 0)$. Figure 2 depicts two orbits projected into the meridional plane. Both were calculated from the same initial data, one adopting the Galactic potential (eqs. [1] and [2]), the other the thin-disk approximation to this potential. The latter simply tends to square up the orbit, which is acceptable provided that the height of the star above the Galactic plane is always much smaller than its distance from the Galactic center.[3]

The thin-disk approximation provides the three isolating integrals of motion, and so the equilibrium phase space distribution function is given by

$$\int dR\, dz\, dv_R\, dv_\phi\, dv_z\, f_{\rm eq}(L_z, E_R, E_z) = \int dR_i\, dz_i\, dv_{Ri}\, dv_{\phi i}\, dv_{zi}\, f_i(R_i, z_i, v_{Ri}, v_{\phi i}, v_{zi}), \quad (6)$$

where the integrals are taken over the regions of phase space around given values of L_z, E_R, and E_z. Changing the integration variables R, v_R, and v_z to these three integrals of motion, we find

$$f_{\rm eq}(L_z, E_R, E_z) = \left[\int_0^{z_{\rm max}} dz_i \int_{v_{\phi\,\rm min}}^{v_{\phi\,\rm max}} dv_{\phi i} \frac{f_i(R_i, z_i, v_{Ri}, v_{\phi i}, v_{zi})}{v_{Ri}\, v_{\phi i}\, v_{zi}}\right] \times \left(\int_0^{z_{\rm max}} dz_i \int_{v_{\phi\,\rm min}}^{v_{\phi\,\rm max}} dv_{\phi i} \frac{1}{v_{Ri}\, v_{\phi i}\, v_{zi}}\right)^{-1}, \quad (7)$$

[3] The thin-disk approximation could be further improved to model the radial variation in the vertical envelope of the orbit by using the vertical action $(2\pi)^{-1}\oint v_z\, dz$, calculated from $\Phi(R, z)$ at each R, as an isolating integral (S. Tremaine 1992, private communication; cf. p. 181 of Binney & Tremaine 1987). In practice, E_z is simpler to use and is adequate for the present application.

© American Astronomical Society • Provided by the NASA Astrophysics Data System

1993ApJ...403..690B

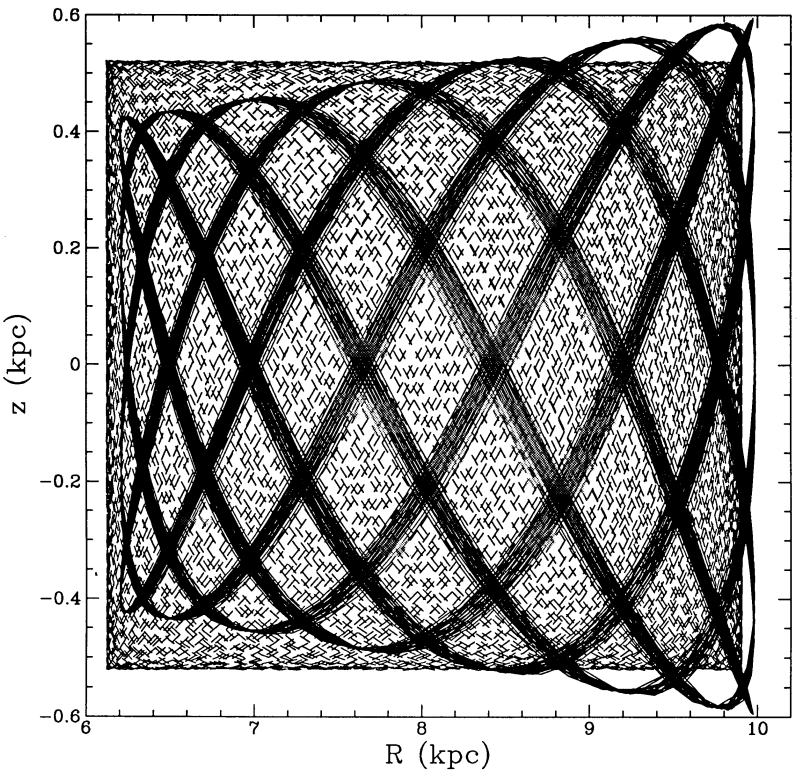

FIG. 2.—Meridional projection of orbit calculated in exact potential (*continuous curve*), and the thin-disk approximation (*dashed curve*). Both orbits were integrated for 10^{10} yr and started from the same initial conditions: $R_i = R_0 = 8.5$ kpc, $z_i = 0$, $v_{Ri} = 66$ km s^{-1}, $v_{\phi i} = 198$ km s^{-1}, and $v_{zi} = 38$ km s^{-1}.

where

$$R_i = L_z/v_{\phi i} , \tag{8}$$

$$v_{Ri} = 2^{1/2}[E_R - v_{\phi i}^2/2 - \Phi(R_i, 0)]^{1/2} , \tag{9}$$

$$v_{zi} = 2^{1/2}[E_z - \Phi(R_0, z_i)]^{1/2} , \tag{10}$$

and the integration limits (representing the bounds to an orbit with these three constants of motion) are given by $E_z = \Phi(R_0, z_{\max})$ and $E_R = 0.5v_{\phi\,\min,\max}^2 + \Phi(L_z/v_{\phi\,\min,\max}, 0)$.

The birth distribution function for the Monte Carlo simulation of the previous subsection is simply the product of equations (3)–(5), $f_i = p(R_i)p(z_i)p(v_{Ri}, v_{\phi i}, v_{zi})$. Adopting this expression, along with the Galactic potential in equations (1) and (2), we find using equation (7) that, at $R = R_0$, $\langle v_R^2\rangle^{1/2} \simeq 69$ km s^{-1}, $\langle[v_\phi - v_g(R_0)]^2\rangle^{1/2} \simeq 48$ km s^{-1}, $\langle v_z^2\rangle^{1/2} \simeq 38$ km s^{-1} (averaged over all heights), $\langle v_\phi - v_g(R_0)\rangle \simeq -7$ km s^{-1}, $\langle z^2\rangle^{1/2} \simeq 670$ pc, and $z_{1/2} \simeq 300$ pc. These numbers are in excellent agreement with the Monte Carlo results, the largest discrepancy being in the asymmetric drift. Moreover, we find that the number density of NSs at $R = R_0$ and $z = 0$ is $n_{\rm NS}^{\rm F} = 1.0 \times 10^{-12} N_{\rm tot}^{\rm F}$ pc^{-3}, perfectly consistent with the Monte Carlo value.

Figure 1 compares the equilibrium speed distributions at $R = R_0$ and $z = 200$ pc calculated from equation (7) with the Monte Carlo results. The thin-disk approximation yields $\langle v\rangle = 82$ km s^{-1} and $\langle v^2\rangle^{1/2} = 92$ km s^{-1} for $z = 200$ pc. The agreement is again remarkable.

2.3. *The Present Local Distribution of Old Neutron Stars*

The thin-disk approximation is much less time-consuming than running a full Monte Carlo simulation, and we shall assume that it is generally valid for all NSs in the disk. For the remainder of the paper we shall adopt the birth parameters of NO's "model b" F and S pulsars and assume that the stars move in the Galactic potential described by equations (1) and (2). Further possibilities for the pulsar distribution function and uncertainties in the Galactic potential could also be explored easily using the thin-disk approximation.

The birth distributions are again given by equations (3)–(5), combined with NO's initial magnetic field distribution,

$$p(\log_{10} B_i) = \frac{1}{C} \exp\left[-\frac{(\log_{10} B_i - \log_{10} B_0)^2}{2\sigma_B^2}\right], \tag{11}$$

and their prescription for relating this to the velocity distribution,

$$\sigma_v = v_0 + v'(\log_{10} B_i - 12.6) . \tag{12}$$

The NO parameters for the F population are $\log_{10} B_0 = 12.61$, $\sigma_B = 0.38$, $v_0 = 60$ km s^{-1}, $v' = 76$ km s^{-1}, and $\sigma_z = 150$ pc. The S population has $\log_{10} B_0 = 12.30$, $\sigma_B = 0.23$, $v_0 = 243$ km s^{-1}, $v' = 260$ km s^{-1}, and $\sigma_z = 450$ pc. The requirement $\sigma_v > 0$ implies that the distribution (11) must be truncated for $\log_{10} B_0 < 11.81$ (11.67) for F (S) stars. Normalizing equation (11) to unit total probability in $\log_{10} B_i$ then implies that $C = 0.936$ and 0.575 for the F and S populations, respectively (both values are close to the true Gaussian value $2^{1/2}\pi^{1/2}\sigma_B$).

According to NO, the current Galactic pulsar birthrates are once every 212 yr and once every 260 yr for the F and S populations, respectively. A constant birthrate therefore implies that there are $N_{\rm tot} \simeq 10^8$ NSs in the Galaxy today. This value is, however, very uncertain, since the birthrate may have been higher in the past. Nucleosynthesis constraints on Galactic chemical evolution require $N_{\rm tot}$ to be as high as 10^9 (Arnett, Schramm, & Truran 1989). Throughout this paper we will

© American Astronomical Society • Provided by the NASA Astrophysics Data System

1993ApJ...403..690B

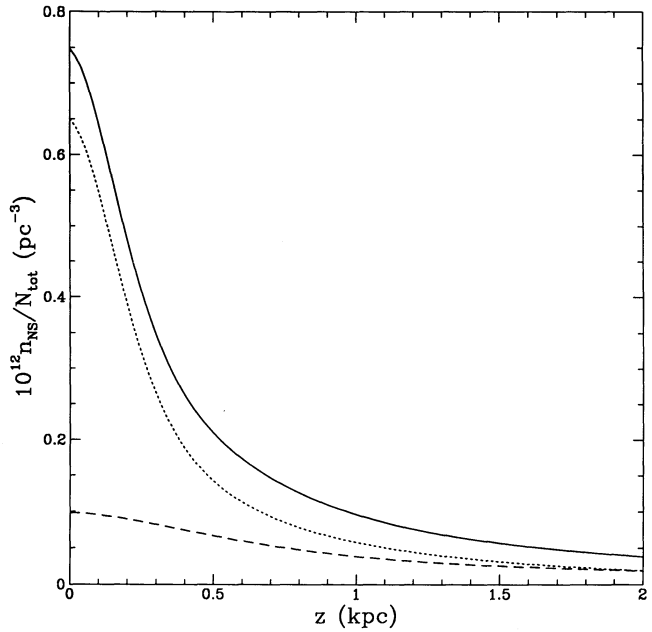

FIG. 3.—Neutron star number density as a function of height at the solar circle $R = R_0$, according to the thin-disk approximation and the NO birth distribution. The solid curve is the total stellar density, while the short-dashed and long-dashed curves depict the contributions of the F and S populations, respectively.

scale all NS numbers with N_{tot} and assume, for simplicity, that the fraction of stars born in each group is independent of birthrate. Hence $N_{tot}^F = 0.55N_{tot}$, and $N_{tot}^S = 0.45N_{tot}$ (NO). Note that, although the S population has a comparable birthrate, it will also have a substantially larger virialized scale height and velocity dispersion (FHP). As a consequence, it will accrete much less matter on average than the F population.

Figures 3 and 4 depict the overall NS height and speed distributions, according to the thin-disk approximation. Because they spend most of their time far out in the Galactic halo, the higher velocity S stars contribute very little to the local NS density, which is

$$n_{NS} = 7.5 \times 10^{-13} N_{tot} \text{ pc}^{-3} . \quad (13)$$

Note that if N_{tot} is as high as 10^9, the nearest NS is expected to be $\lesssim 7$ pc from the Sun. The column density of NSs through the Galactic plane is

$$\Sigma_{NS} = 7.0 \times 10^{-10} N_{tot} \text{ pc}^{-2} . \quad (14)$$

The height distribution of Figure 3 has

$$z_{1/2} = 280 \text{ pc} \quad (15)$$

and

$$\langle z^2 \rangle^{1/2} = 710 \text{ pc} . \quad (16)$$

The derived half-density NS scale height is in good agreement with the estimates made by FHP using a different Galactic potential. It is important to stress that this scale height is much larger than that observed for Population I objects (~ 50 pc), approximately twice as large as that of neutral atomic hydrogen, and comparable to those of G, K, and M stars.

From Figure 4*b* we see that, at $z = 0$, 6% of NSs have $v \leq 20$ km s^{-1}, 22% have $v \leq 40$ km s^{-1}, 50% have $v \leq 72$ km s^{-1}, and 70% have $v \leq 106$ km s^{-1}. The mean and rms speeds are

$$\langle v \rangle = 81 \text{ km s}^{-1} \quad (17)$$

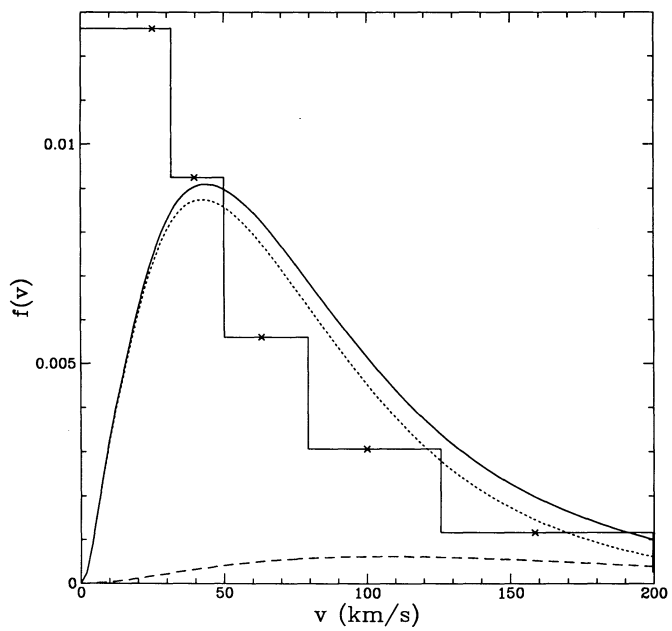

FIG. 4*a*

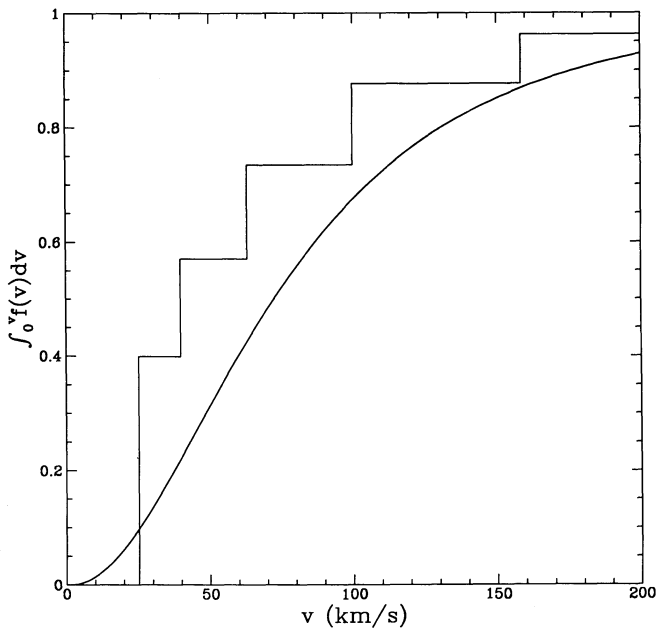

FIG. 4*b*

FIG. 4.—(*a*) Differential neutron star speed distribution at $R = R_0$, $z = 0$, normalized to unit area. The distribution was calculated according to the thin-disk approximation and the NO birth distribution. The solid curve is the total distribution, while the short-dashed and long-dashed curves depict the contributions of the F and S populations, respectively. For comparison, the distribution used by TC is also shown. This is a set of delta functions at the points indicated, with the area contributed by each velocity given by the area in the corresponding bin. (*b*) Total cumulative speed distribution from the thin-disk approximation (*smooth curve*) and as used by TC (*histogram*).

© American Astronomical Society • Provided by the NASA Astrophysics Data System

1993ApJ...403..690B

and

$$\langle v^2 \rangle^{1/2} = 98 \text{ km s}^{-1} , \quad (18)$$

respectively. For comparison, the combined F and S birth speed distribution of NO has $\langle v_i \rangle = 172$ km s^{-1} and $\langle v_i^2 \rangle^{1/2} = 218$ km s^{-1}. Thus, close to the Galactic plane, the fraction of relatively low-velocity NSs at equilibrium is much larger than at birth. The values in equations (13)–(18) do not differ greatly from the results of the previous two subsections, even though both the S population and a distribution of initial magnetic field strengths are now included. A polynomial fit,

$$f(v) = \sum_{j=0}^{6} c(j) v^j ,$$

to the differential speed distribution plotted in Figure 4*a* yields $c(j, j = 0, 6) = (-1.026 \times 10^{-3}, 5.572 \times 10^{-4}, -1.071 \times 10^{-5}, 8.630 \times 10^{-8}, -3.531 \times 10^{-10}, 7.218 \times 10^{-13}, -5.836 \times 10^{-16})$. The fit can be applied over the range $4 \leq v \leq 270$ km s^{-1}, with a maximum error of order 15%.

Figure 4 also depicts the speed distribution adopted by TC, which clearly has more low-velocity (corresponding to higher accretion rates) NSs than ours. TC's distribution is somewhat problematic, since it is based on Monte Carlo simulation results of Paczyński (1990), who stated how many stars currently located in the solar neighborhood were *born* with a given velocity. Hence the velocities for each of TC's bins are really birth velocities for that population of stars. It is not clear how this distribution relates to the actual current speed distribution of stars, given that their velocities vary with time on their orbital paths. Stars born with low peculiar velocities will continue to have low speeds, however, so TC's low-velocity bin is probably reasonable, and its size reflects an excess number of low-velocity stars in Paczyński's (1990) birth distribution as compared with that of NO. We discuss the differences in predicted numbers of detectable sources produced by the two speed distributions in § 5 below.

We have not attempted to calculate the detailed kinematic properties of NSs which are born with sufficiently large velocities to send them out into the Galactic halo. We can, however, estimate their number by assuming that they start with $v_i > v_g(R_0) = 220$ km s^{-1}. The NO birth distributions then imply that $N_{\text{halo}} \simeq 0.28 N_{\text{tot}}$, that is, roughly one-third of all NSs born in the Galactic disk will end up in a halo population.

3. GEOGRAPHY OF THE INTERSTELLAR MEDIUM

A discussion of the properties of the accreting sources, and a study of the detectability of isolated NSs in the solar neighborhood, require a detailed mapping of the local ISM.

3.1. *The Local Interstellar Medium*

The morphology and physical state of the plasma in the local interstellar medium (LISM), at distances $\lesssim 1$ kpc, is currently a very active field of research (for recent reviews see, e.g., Bochkarev 1987; Bruhweiler & Vidal-Madjar 1987; Cox & Reynolds 1987; Frisch & York 1991). The solar system is embedded in warm (~ 8000 K), low-density (~ 0.1 cm^{-3}) partially ionized gas. This "local fluff" only extends out to a distance of several parsecs and is therefore unlikely to contain any NSs given the expected space density. For distances ~ 100 pc beyond this, interstellar absorption measurements (summarized by Paresce 1984) suggest that the solar system is embedded in an anomalously low-density region. This is widely believed to contain hot ($\sim 10^6$ K), low-density ($\sim 5 \times 10^{-3}$ cm^{-3}) plasma giving rise to the extreme ultraviolet/soft X-ray (EUV/SXR) background. A recent simple model by Snowden et al. (1990) assumes that this plasma is uniform inside an irregular "local bubble" which is completely devoid of neutral material. They deduce an X-ray emission volume of $\sim 10^7$ pc^3, implying that there could be as many as 10^4 NSs inside the bubble. Unfortunately, the maximum accretion rate from the hot plasma is only $\sim 5 \times 10^6$ g s^{-1}, far too low to be observable.

However, in addition to the local fluff, higher density diffuse atomic and molecular clouds are known to exist within this region (see, e.g., Frisch & York 1991 for the nearest ones). Such clouds would allow NSs to accrete at much higher rates. The total number of clouds within the local bubble is still unknown, but observations in the Be band (covering $\sim 10\%$ of the sky) apparently permit a filling factor of up to 25% for local fluff type cloudlets (Juda et al. 1991). In fact, the interstellar absorption measurements suggest the rather ubiquitous presence of smoothly distributed neutral gas with $n_{\text{H}} \sim 0.07$ cm^{-3} and temperature $\sim 10^3$–10^4 K (Paresce 1984). In the Galactic plane directions $270° < l < 15°$ and $120° < l < 200°$, this gas extends out to ~ 100 pc. For $200° < l < 270°$, the interstellar medium is devoid of neutral gas to great distances ~ 200 pc. Even in this direction, somewhat hotter ionized gas with comparable density still fills a substantial volume (Gry, York, & Vidal-Madjar 1985). Finally, in the range $15° < l < 120°$ there is apparently an H I wall with $n_{\text{H}} \sim 1$ cm^{-3} at a distance of $\lesssim 16$ pc, with very little H I beyond 50 pc. Additional H I walls with $n_{\text{H}} \sim 1$–10 cm^{-3} exist, particularly in the direction of radio Loop I ($l = 330°$) at low Galactic latitude ($b \lesssim 40°$) and at a distance of ~ 100 pc (Iwan 1980). The Loop I bubble itself is filled with low-density coronal gas.

3.2. *Giant Molecular Clouds*

The highest accretion rates will occur on NSs in giant molecular clouds (GMCs), the nearest of which are summarized by Dame et al. (1987). Table 1 lists the clouds along with their distances and the expected number of NSs per cloud. The latter

TABLE 1

NEUTRON STARS IN GIANT MOLECULAR CLOUDS

Region	Distance (pc)	Number ($N_{\text{tot}} = 10^9$)
Aquila rift	200	20
Cloud A	500	3
Cloud B	300	3
Cloud C	500	2
Vulpecula rift	400	8
Cygnus rift	700	300
Cygnus OB7	800	240
Lindblad ring	300	20
"-12 km s^{-1}"	800	300
Cepheus	450	30
Taurus	140	2
Perseus OB2	350	20
Monoceros OB1	800	20
Orion A	500	20
Orion B	500	30
Monoceros R2	830	20
Vela sheet	425	8
Lupus	170	2
ρ Oph	165	2

© American Astronomical Society • Provided by the NASA Astrophysics Data System

1993ApJ...403..690B

was computed by using the GMC "condensation" law, which relates the mean molecular number density $n_{\rm mol}$ to the radius $R_{\rm cl}$ (in pc) of the cloud,

$$n_{\rm mol} = 1700 R_{\rm cl}^{-1}\ {\rm cm}^{-3}\ . \tag{19}$$

We took the numerical constant in this relation from the data presented by Myers & Goodman (1988), which they showed could be adequately fitted by a 30 μG magnetic equilibrium. Adopting spherical clouds with a mean molecular mass of $2.33 m_p$, equation (19) implies that the number of NSs in a particular cloud of mass $M_{\rm cl}$ is

$$N_{\rm NS} = 5 \times 10^{-4} \left(\frac{n_{\rm NS}}{\rm pc^{-3}}\right)\left(\frac{M_{\rm cl}}{M_\odot}\right)^{3/2}\ . \tag{20}$$

The molecular cloud data have a large scatter about equation (19), and so our NS numbers in Table 1 are meant to be indicative only. (Roughly, they might be too low by a factor of 15 or too high by a factor of 6.) To help gauge the uncertainties, we consider the Taurus-Auriga complex (the closest GMC at a distance of $d = 140$ pc) in some detail. From Table 2 of Ungerechts & Thaddeus (1987), the total solid angle of this complex on the sky is $\Omega_{\rm cl} = 0.071$ sr, which corresponds to a volume [defined as $4\Omega_{\rm cl}^{3/2} d^3/(3\pi^{1/2})$]$V_{\rm cl} = 3.9 \times 10^4$ pc^3. For comparison, equation (20) implies a cloud volume of only 3.3×10^3 pc^3 when the total mass of the complex inferred from CO measurements, $M_{\rm cl} = 3.5 \times 10^4\ M_\odot$, is inserted. This is consistent with the observed scatter in the condensation law (eq. [19]), and it implies that the total number of NSs in this complex is ~ 30 rather than ~ 2 as stated in Table 1. We note, however, that Taurus-Auriga, like most GMCs, is not spherical, and so this number is still somewhat uncertain.

Very high accretion rates could be achieved in GMC cores, which can have densities in excess of 10^8 cm^{-3} (e.g., Turner 1988). Thus even relatively high-velocity NSs can have accretion rates at least as large, and perhaps much higher, than those of low-velocity NSs in the average interstellar medium. However, cores have a very small filling factor, and few NSs are expected to reside in them.

4. ACCRETION STATISTICS

The instantaneous accretion rate onto the surface of a NS is described by the Bondi formula:

$$\dot{M} = \frac{4\pi\lambda_a G^2 M^2 \rho}{(v^2 + c_s^2)^{3/2}}\ , \tag{21}$$

where M is the star mass, v is the relative speed between the NS and the interstellar medium, c_s is the ambient sound speed, and ρ is the ambient interstellar mass density. The parameter λ_a varies from 0.25 for $v \ll c_s$ to unity for $v \to \infty$ (Hunt 1971). Throughout this paper we assume $\lambda_a = 1$ for a representative NS of mass $M = 1.4\ M_\odot$, radius $R = 10$ km, and surface gravity $g = 2 \times 10^{14}$ cm s^{-2}. We choose $c_s = 10$ km s^{-1}, typical for a photoionized gas at 8000 K. (The exact value of the sound speed affects only the high-$\dot{M}$ tail of the distribution.) Note that the range of local NS speeds from Figure 4 produces an effect in equation (21) comparable to the range of local interstellar densities, and so both are equally important in determining the accretion rate distribution.

4.1. *Do Isolated Neutron Stars Accrete?*

If the NS is magnetized and spinning rapidly, then radiation pressure and the rotating magnetic field can each prevent potentially accreted material from reaching the surface of the star (e.g., Ostriker et al. 1970; Illarionov & Sunyaev 1975; Davies & Pringle 1981; Bhatt 1990; Blaes et al. 1992). These two barriers can drastically reduce the number of observable NSs, and different authors reach different conclusions, depending primarily on the way they treat the "propeller mechanism" for NS spindown. We therefore review the problem here.

Consider a NS with a dipolar field $B = 10^{12} B_{12}$ G, a rotation period P s, and a speed relative to the ISM $v = 40 v_{40}$ km s^{-1}, which is slowing down at the magnetic dipole rate. First, accretion can proceed if the ram pressure of the incoming gas at the accretion radius,

$$r_B \sim \frac{GM}{v^2} \simeq 10^{13} v_{40}^{-2}\ {\rm cm}\ , \tag{22}$$

exceeds the pulsar momentum flux. This requires the NS to be spun down to

$$P \gtrsim P_B \simeq 9 B_{12}^{1/2} n^{-1/4} v_{40}^{1/2}\ {\rm s}\ , \tag{23}$$

where n is the nucleon number density in the ambient gas. This takes

$$t_B \simeq 5 B_{12}^{-1} n^{-1/2} v_{40}\ {\rm Gyr} \tag{24}$$

to occur. Given that this is an order-of-magnitude estimate, t_B is uncomfortably close to the age of the Galaxy for the parameter values chosen. Nevertheless, if the estimate is taken literally, then the speed distribution of Figure 4*b* implies that roughly half of all local NSs can spin down sufficiently to overcome this first barrier, at least if the majority of them were born early on in the history of the Galaxy. Note that t_B is inversely proportional to B, so that field strengths greater than 10^{12} G (NO find $\simeq 4 \times 10^{12}$ G for the locally dominant F population; see § 2.3 above) further increase this fraction.

Equation (24) assumes that the NS magnetic fields are constant in time, but observations of pulsars seem to suggest that they decay with a time scale $\lesssim 10^7$ yr (Lyne, Manchester, & Taylor 1985), and NO's best-fit model has an exponential decay with e-folding time 1.3×10^7 yr. There is some evidence for a long-lived "residual" component $B_f \lesssim 10^{10}$ G (Kulkarni 1986), at least for NSs in binaries. More recently, Bhattacharya et al. (1992) have argued that the observations are in fact best fitted if no significant field decay occurs in single radio pulsars over 10^8 yr time scales.

Magnetic field evolution will affect the previous estimates in the following way. From equation (24), a constant field of $B_{12} \lesssim 0.5 n^{-1/2} v_{40}$ will not be able to slow down an initially rapidly spinning NS sufficiently. If a NS is born with a higher field strength B_i which then decays, then the pulsar wind can be overcome if the decay time scale exceeds the time scale required to reach the critical period P_B associated with the residual field strength B_f. The latter is given by a small modification of equation (24),

$$t_B' \simeq 5 B_{i12}^{-2} B_{f12} n^{-1/2} v_{40}\ {\rm Gyr}\ . \tag{25}$$

For example, with the adopted scalings for B_i, v, and n, a residual field strength of 10^9 G requires a field decay time scale $\gtrsim 10^7$ yr for the inflow to proceed inside r_B.

Once the gas can penetrate the accretion radius, it will not be obstructed until the NS magnetic pressure can balance the

© American Astronomical Society • Provided by the NASA Astrophysics Data System

1993ApJ...403..690B

ram pressure at the Alfvén radius,[4]

$$r_A \simeq 3 \times 10^{10} B_{12}^{4/7} n^{-2/7} v_{40}^{6/7} \text{ cm} . \quad (26)$$

This lies just inside the light cylinder $cP_B/(2\pi)$ for $v_{40} \lesssim 2n^{1/10}B_{12}^{-1/5}$. The corotating magnetosphere will then prevent accretion unless the NS has spun down to the orbital period at r_A,

$$P_C \simeq 3 \times 10^{3} B_{12}^{6/7} n^{-3/7} v_{40}^{9/7} \text{ s} . \quad (27)$$

This greatly exceeds the period (23) which can be reached by magnetic dipole radiation. The accreted material will however, be spun up by the magnetosphere and therefore exert a torque of its own on the NS. Unfortunately this interaction between the magnetosphere and the plasma is poorly understood (cf. Davies, Fabian, & Pringle 1979), and probably requires a full three-dimensional numerical simulation. In terms of allowing accretion, the most pessimistic estimate (Illarionov & Sunyaev 1975) proposes that the magnetosphere acts as a "propeller" which shock heats and expells all the incoming material. Neglecting cooling, energy conservation then implies a torque $\sim GM\dot{M}/(r_A\Omega)$, giving a spin-down time from $P = P_B$ of $\sim 100 B_{12}^{-3/7} n^{-11/14} v_{40}^{20/7}$ Gyr, which is far too long except for the low-velocity tail of the NS speed distribution. If, on the other hand, the material can cool, then it must be spun up to Keplerian rotation rates in order to be expelled. The torque would then have to be $\sim \dot{M}(GMr_A)^{1/2}$, giving a spin-down time scale $\sim 0.8 B_{12}^{-11/14} n^{-17/28} v_{40}^{29/14}$ Gyr, perfectly adequate to allow interstellar accretion. Numerical simulations by Wang & Robertson (1985) indicate that even more rapid spin-down may occur if the accreted material can build up, compressing the magnetosphere and becoming unstable to large-scale mixing with the magnetic field. Because the time scales generally increase with decreasing B, field decay affects the propeller in the same way as it affects the pulsar's magnetic dipole spin-down.

Finally, equation (21) assumes that the accretion flow is hydrodynamic, which is true only if the ambient medium is ionized (Alcock & Illarionov 1980). Otherwise the inflow rate is reduced by a factor $\sim r_B/R \simeq 10^7 v_{40}^{-2}$. As we discuss in § 6.1 below, the surface temperature of a NS accreting material at the hydrodynamic rate is sufficient to photoionize the ambient medium and thus provides a self-consistent scenario. However, until the star has spun down and/or the field has decayed sufficiently to allow accretion, the only material which can be used to provide a torque in the propeller mechanism will come from the warm ionized medium. This phase apparently has a large volume filling factor, and so our estimates should not be altered too much.

From the discussion above, it is then likely that a large fraction of the entire NS population is currently accreting material from the ISM. Keeping in mind the above uncertainties, we shall assume in the following sections that all old local NSs do in fact accrete at the Bondi rate.

4.2. *Accretion Rate Distribution*

Figure 5 shows the cumulative distribution of accretion rates for the F + S NS population in a medium of density 100 cm^{-3}. We derive $\langle \dot{M} \rangle \simeq 10^{12.25}$ g s^{-1}; 6% of NSs are found to accrete at $\dot{M} \geq 10^{12.8}$ g s^{-1}, 22% at $\dot{M} \geq 10^{12}$ g s^{-1}, 50% at $\dot{M} \geq 10^{11.3}$ g s^{-1}, and 70% at $\dot{M} \geq 10^{10.8}$ g s^{-1}. The maximum rate corresponds to $v = 0$, and is as large as $10^{13.9}$ g s^{-1}. The plotted curve may be shifted horizontally for different values of n and stellar mass M, according to $\dot{M} \propto M^2 n$. The mean accretion rate in the average ISM ($n \sim 1$ cm^{-3}) is therefore $\langle \dot{M} \rangle_{\rm ISM} \simeq 10^{10.25}$ g s^{-1}. Note that, since the first moment of the high-$\dot{M}$ tail of the distribution is large, the mean fails as an estimator of the central value. More information is actually provided by the median value.

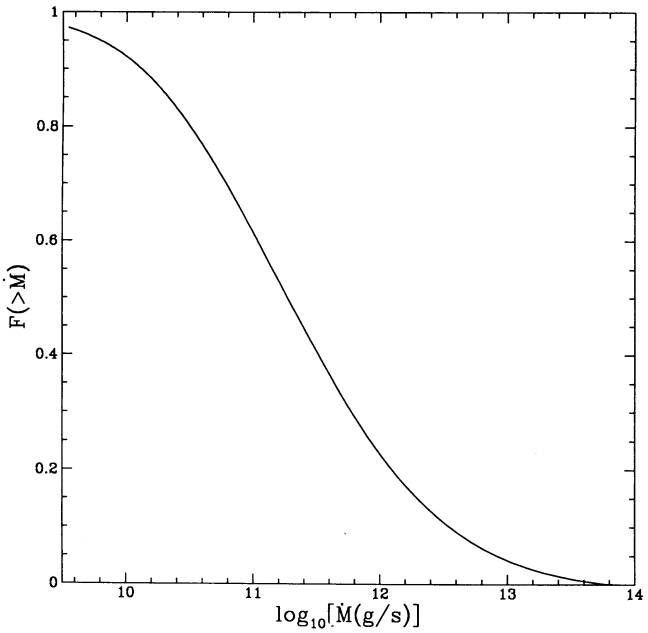

FIG. 5.—Cumulative distribution of accretion rates for neutron stars moving in a medium with $n = 100$ cm^{-3}.

4.3. *Quiescent Emission Properties*

As infalling protons dissipate their kinetic energy at the NS surface and liberate $\simeq 200$ MeV nucleon^{-1}, the total luminosity radiated is $L \simeq 1.9 \times 10^{30} \dot{M}_{10}$ ergs s^{-1}, where $\dot{M}_{10}$ is the accretion rate in units of 10^{10} g s^{-1}. The effective blackbody surface temperature is then

$$T_{\rm BB} \simeq 20 \dot{M}_{10}^{1/4} f^{-1/4} \text{ eV} , \quad (28)$$

where f is the fraction of the star's surface on which gas accretes. The radiation spectrum resulting from accretion depends on the flow geometry and on the detailed manner in which the incident gas is decelerated and thermalized near the NS surface. In the absence of collective effects, the incident ions are slowed down by Coulomb collisions (Zel'dovich & Shakura 1969). The Coulomb stopping length is ~ 5–10 Thomson-scattering mean free paths into the atmosphere, and the emergent radiation is essentially a Planck curve at $T \simeq T_{\rm BB}$. On the other hand, if plasma instabilities can arise and grow rapidly, the proton mean free path might be reduced below the collisional stopping length and a stationary, collisionless shock would form near the stellar surface. In this alternative scenario, high-energy radiation at $T \gg T_{\rm BB}$ is emitted in a layer between the shock discontinuity and the surface (Shapiro & Salpeter 1975). Langer & Rappaport (1982) have investigated this mechanism in the case of highly magnetized NSs, where cyclotron emission is the dominant cooling process. Most recently Nelson, Salpeter, & Wasserman (1992) have argued that, as

[4] Note that this second barrier does indeed lie inside the accretion radius for the vast majority of local NSs which satisfy $v_{40} \lesssim 8n^{1/10}B_{12}^{-1/5}$. See, e.g., Harding & Leventhal (1992) for accretion in the opposite regime.

© American Astronomical Society • Provided by the NASA Astrophysics Data System

1993ApJ...403..690B

freely falling protons excite electron Landau transitions in the magnetized atmosphere of accreting NSs, a significant fraction, $f_x \simeq 0.1 B_{12}^{7/6}$, of the total accretion luminosity should be emitted just below the cyclotron energy $E_B = 11.6 B_{12}$ keV. This nonthermal high-energy feature, smeared out by Compton scattering, would appear superposed on the Wien tail of the much lower energy thermal spectrum (Nelson et al. 1992).

The largest complication introduced by the presence of a magnetic field is in the large-scale topology of the accretion flow onto the polar cap. The problem of how the spherically infalling plasma enters the magnetosphere of a strongly magnetized NS is not fully resolved. In the kinematic model, one simply assumes that the incoming material is channeled to the poles by those field lines which would have passed beyond the Alfvén radius (Davidson & Ostriker 1973). The cross-sectional area of the accretion column is then $\sim 10^8 B_{12}^{-4/7} \dot{M}_{10}^{2/7}$ cm^2. Alternatively, percolation of plasma blobs between field lines (via a Rayleigh-Taylor instability) has been suggested to mediate the accretion flow. This model yields a much larger value for the polar cap area (Arons & Lea 1980); in particular, when the accretion rate is small, the material is found to land over the entire star surface. If the accretion columns have a total cross-sectional area $A = A_1$ km^2, the effective temperature of the polar caps is

$$T_{\rm BB} \simeq 120 \dot{M}_{10}^{1/4} A_1^{-1/4} \text{ eV} . \quad (29)$$

It is worth remarking that cooling curves (Nomoto & Tsuruta 1987) show that the surface temperature of a NS will drop below 20 eV in $t_{\rm cool} \sim 10^6$ yr. The accretion of interstellar material will therefore maintain the surface of old NSs at several hundred thousand degrees even for $t \gg t_{\rm cool}$.

In the following, we will discuss the emission properties and detectability of NSs accreting material mainly from three different gas phases: the local cavity, with $n = 0.07$ cm^{-3}; the ISM, with a local volume average density $n = 1$ cm^{-3}; and diffuse molecular clouds, with $n = 100$ cm^{-3}. Table 2 lists the corresponding maximum and median accretion rates, effective temperatures, specific luminosities at 100 Å, and soft X-ray luminosities in the *ROSAT* 0.1–2.4 keV band, in the case of isotropic and polar cap accretion. It is clear that the results of our investigation will be sensitive to the (unknown) flow topology in the NS magnetosphere. If the emitted spectrum is Planckian, then in the Rayleigh-Jeans regime the luminosity per unit frequency radiated by an isotropically accreting NS will always be larger than the corresponding luminosity radiated by a polar cap accretor. The contrary will be true in the Wien regime, provided

$$\frac{h\nu}{kT_{\rm BB}^{\rm cap}} \gtrsim -\frac{f^{1/4} \ln f}{1 - f^{1/4}} , \quad (30)$$

where all symbols have their usual meanings. The right-hand side of this inequality never exceeds 4 for all $f < 1$.

TABLE 2

PROPERTIES OF ACCRETING NEUTRON STARS[a]

Property	$n = 0.07$ cm^{-3}	$n = 1$ cm^{-3}	$n = 100$ cm^{-3}
$\dot{M}_{\rm max}$	5.1 (10)	7.3 (11)	7.3 (13)
$\langle \dot{M} \rangle$	1.2 (09)	1.7 (10)	1.7 (12)
$\dot{M}_{\rm med}$	1.3 (08)	1.9 (09)	1.9 (11)
$T_{\rm BB,\,max}^{\rm iso}$	29	57	180
$T_{\rm BB,\,max}^{\rm cap}$	170	340	1100
$T_{\rm BB,\,med}^{\rm iso}$	6.6	13	41
$T_{\rm BB,\,med}^{\rm cap}$	39	76	240
$L_{\rm max}^{\rm iso}$(100 Å)	2.3 (14)	2.0 (15)	1.6 (16)
$L_{\rm max}^{\rm cap}$(100 Å)	1.2 (13)	2.8 (13)	1.0 (14)
$L_{\rm med}^{\rm iso}$(100 Å)	1.1 (08)	1.0 (12)	7.8 (14)
$L_{\rm med}^{\rm cap}$(100 Å)	5.6 (11)	3.1 (12)	1.9 (13)
$L_{\rm max}^{\rm iso}$(0.1–2.4 keV)	4.9 (30)	1.2 (32)	1.3 (34)
$L_{\rm max}^{\rm cap}$(0.1–2.4 keV)	9.4 (30)	1.3 (32)	3.1 (33)
$L_{\rm med}^{\rm iso}$(0.1–2.4 keV)	4.3 (24)	1.6 (28)	2.5 (31)
$L_{\rm med}^{\rm cap}$(0.1–2.4 keV)	1.7 (28)	3.3 (29)	3.5 (31)

[a] Units: $\dot{M}$: g s^{-1}; $T_{\rm BB}$: eV; L(100 Å): ergs s^{-1} Hz^{-1}; and L(0.1–2.4 keV): ergs s^{-1}. Numbers in the case of polar cap accretion are given for $A_1 = 1$. Quantities indicated with the subscript "max" are computed in the $v = 0$ limit; the subscript "med" indicates median values.

5. THE OBSERVABILITY OF ACCRETING, ISOLATED NEUTRON STARS

5.1. *Constraints from a Search for Stellar Soft X-Ray Sources*

A search for soft (<280 eV) radiation from individual stellar sources was carried out as part of the *Skylab* program (Vanderhill et al. 1975). The survey covered about one-tenth of the sky with a sensitivity $S_{\rm min} \simeq 10^{-27}$ ergs s^{-1} cm^{-2} Hz^{-1} at 0.26 keV, and revealed no evidence for soft X-ray emission from stellar sources. We can use this null detection to put an upper limit to the local NS density, assumed here to be constant. The integrated source counts can be calculated as

$$N(>S) = \frac{\Omega n_{\rm NS}}{24\pi^{3/2}} \langle L^{3/2} \rangle S^{-3/2} , \quad (31)$$

where $\Omega/4\pi$ is the fraction of the sky covered by the survey, and the average is taken over the luminosity distribution. In the best case of accretion onto the polar cap with $A_1 = 1$, the maximum luminosity at 0.26 keV of a NS accreting material in the local cavity is $L_{\rm max}^{\rm cap}(0.26 \text{ keV}) \simeq 3 \times 10^{13}$ ergs s^{-1} Hz^{-1}. The sampling depth is then $d_{\rm max} = [L_{\rm max}^{\rm cap}/(4\pi S_{\rm min})]^{1/2} \simeq 17$ pc, well inside the cavity. We also derive $\langle L^{3/2}(0.26 \text{ keV}) \rangle^{2/3} \simeq 3 \times 10^{12}$ ergs s^{-1} Hz^{-1}. This yields the expected number of observable NSs:

$$N_{\textit{Skylab}}^{\rm cap} \simeq 50 \left(\frac{n_{\rm NS}}{\text{pc}^{-3}} \right) , \quad (32)$$

which, when compared with the fact that no stellar sources were actually detected, implies $n_{\rm NS} < 0.02$ pc^{-3}. This is several times less than the Oort limit (0.05 pc^{-3}) allows, and roughly $25(10^9/N_{\rm tot})$ times greater than the expected NS density from equation (13). For isotropic accretion, on the other hand, $\langle L^{3/2}(0.26 \text{ keV}) \rangle^{2/3} \simeq 4 \times 10^{11}$ ergs s^{-1} Hz^{-1}, and even the Oort limit is consistent with no observed sources.

5.2. *The EUVE and ROSAT WFC All-Sky Surveys*

In the first 6 months of the forthcoming *EUVE* mission, an all-sky survey will be carried out covering 90–750 Å in four colors (Bowyer et al. 1991). Its anticipated sensitivity will range from $\sim 10^{-3}$ photons cm^{-2} s^{-1} Å^{-1} at the longest wavelengths to 6×10^{-5} photons cm^{-2} s^{-1} Å^{-1} in the band 90–150 Å. (A deeper survey, with 10–50 times greater sensitivity, will be conducted on a portion of the sky from 90 to 400 Å.) The *ROSAT* wide field camera (WFC) has already completed its all-sky survey in a similar wavelength range (80–200 Å), and is expected to turn up a thousand sources, about two-thirds identifiable with known objects (Pounds et al. 1991). The point-source sensitivity at 100 Å is $\sim 1.5 \times 10^{-5}$ photons cm^{-2} s^{-1} Å^{-1}.

© American Astronomical Society • Provided by the NASA Astrophysics Data System

1993ApJ...403..690B

As we discussed in § 3.1 above, the local interstellar medium has a complex, highly anisotropic geography for which our knowledge is still incomplete. This makes it difficult to estimate the total number of detectable NSs, especially as the interstellar density determines both the intrinsic luminosity of sources (through accretion) and the amount of absorption along the line of sight. For definiteness, we consider here four different possible lines of sight. The first passes through 100 pc of local cavity material ($n = 0.07$ cm^{-3}) and then goes into a surrounding medium with $n = 1$ cm^{-3}. We take all the material along this line of sight to be neutral, so that both accretion and absorption depend on the total particle density. This description should be appropriate for many directions in the Galactic plane, particularly toward radio Loop I (provided our line of sight does not penetrate beyond the H I wall into the interior of this bubble). The second line of sight is the same, except that we take the cavity to extend only to 16 pc, followed by neutral $n = 1$ cm^{-3} gas out to 50 pc, and then no material beyond. This describes the direction toward the nearby H I wall in the region $15° < l < 120°$ discussed by Paresce (1984). The third line of sight goes through $n = 0.07$ cm^{-3} out to great distances. Here we take the material to be fully ionized (implying negligible absorption). This describes the "empty" third quadrant in the Galactic plane. Finally, we consider a fourth line of sight which goes through 100 pc of local cavity and then has no material, and therefore no sources, beyond. This crudely models a direction toward the Galactic poles in which NSs beyond the local scale height of the interstellar medium contribute negligibly to the counts. We assume that the NS space density is constant along all four lines of sight because we never probe beyond the NS scale height.

The number of detectable NSs along a given line of sight is given by

$$\frac{dN}{d\Omega}(>S) = \int_0^\infty dL \int_0^{d(L)} dr\, r^2 p(L, r) n_{\rm NS}\,, \qquad (33)$$

where $p(L, r)$ is the luminosity function of the accreting sources (derived from the accretion rate distribution associated with the ambient interstellar densities), $d(L)$ is the maximum distance that a source of luminosity L could be seen,

$$4\pi d^2(L) S = L \exp\left(-\int_0^{d(L)} dr\, n_{\rm H\,I}\,\sigma\right), \qquad (34)$$

and σ is the absorption cross section which at 100 Å is 3.17×10^{-20} cm^2 (Morrison & McCammon 1983).

The cumulative source counts for each of the four lines of sight are shown in Figure 6. Line of sight 3 through the third quadrant gives a Euclidean slope $N(>S) \propto S^{-3/2}$ because of the constant luminosity function and the lack of absorption. The other lines of sight can have steeper or shallower counts depending on the relative importance of increased intrinsic luminosities in the H I walls, on the one hand, and cutoffs in the interstellar density and absorption, on the other. A momentary steepening in the counts for a line of sight toward an H I wall, such as that depicted for the first line of sight in the isotropic accretion case, is in principle a signature of accreting NSs. In practice, however, it appears that the numbers are too small to make this observable, especially when the background of other EUV/X-ray sources is included.

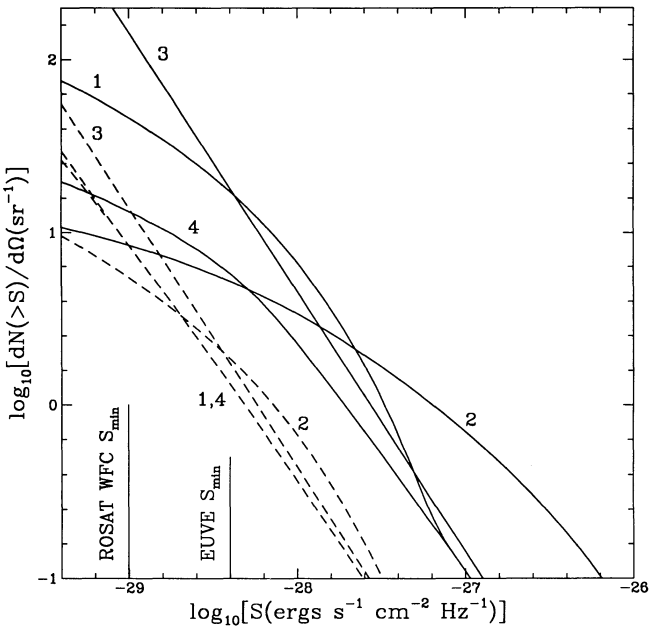

FIG. 6.—Cumulative source counts at 100 Å for the four different lines of sight discussed in the text. Line of sight 1 has neutral material with density 0.07 cm^{-3} inside 100 pc and 1 cm^{-3} beyond. Line of sight 2 is the same, but with the 1 cm^{-3} material starting at 16 pc and finishing at 50 pc, with nothing beyond. Line of sight 3 goes through uniform 0.07 cm^{-3} ionized material. Line of sight 4 is the same as line of sight 1, except that no material exists beyond 100 pc. Solid curves are for isotropic accretion, and dashed curves are for polar cap accretion with $A_1 = 1$. The total number of Galactic neutron stars is taken to be 10^9.

Table 3 gives the predicted number of sources detectable by *EUVE* and the *ROSAT* WFC along each of the four lines of sight, together with the corresponding maximum sampling distances. If we assume that line of sight 1 is typical of the local cavity as a whole, then the total numbers of sources expected in

TABLE 3

PREDICTED NUMBERS OF SOURCES AND SAMPLING DISTANCES

Line of Sight	$dN_{EUVE}/d\Omega$ $[(N_{tot}/10^9)\,sr^{-1}]$	d_{max}^{EUVE} (pc)	$dN_{WFC}/d\Omega$ $[(N_{tot}/10^9)\,sr^{-1}]$	d_{max}^{WFC} (pc)	$dN_{PSPC}/d\Omega$ $[(N_{tot}/10^9)\,sr^{-1}]$	d_{max}^{PSPC} (pc)
1 (isotropic)	17	130	46	140	640	430
2 (isotropic)	5.2	50	8.4	50	...	...
3 (isotropic)	18	220	140	440	...	...
4 (isotropic)	5.8	100	13	100	17	100
1 (polar cap, $A_1 = 1$)	1.3	43	8.5	100	12000	1500
2 (polar cap, $A_1 = 1$)	1.9	33	5.5	42	...	...
3 (polar cap, $A_1 = 1$)	1.8	50	14	100	...	...
4 (polar cap, $A_1 = 1$)	1.3	43	8.4	77	98	100

© American Astronomical Society • Provided by the NASA Astrophysics Data System

1993ApJ...403..690B

each of the two sky surveys are

$$N_{EUVE}^{\rm iso} \simeq 200\left(\frac{N_{\rm tot}}{10^9}\right), \quad (35)$$

$$N_{EUVE}^{\rm cap} \simeq 20\left(\frac{N_{\rm tot}}{10^9}\right), \quad (36)$$

$$N_{\rm WFC}^{\rm iso} \simeq 600\left(\frac{N_{\rm tot}}{10^9}\right), \quad (37)$$

and

$$N_{\rm WFC}^{\rm cap} \simeq 100\left(\frac{N_{\rm tot}}{10^9}\right). \quad (38)$$

We note that equations (37) and (38) are consistent with the number of unidentified sources from the *ROSAT* WFC "minisurvey" (Pounds et al. 1991).

Finally, we note that the very different source counts along each of the lines of sight for the case of isotropic accretion translate into a substantial source anisotropy on the sky. In particular, line of sight 4 (toward a Galactic pole) shows a substantial deficit of sources compared with the Galactic plane lines of sight 1 and 3, indicating a significant concentration of sources toward the Galactic plane. If, however, accretion is confined to the polar caps, then the counts in Table 3 are similar for all lines of sight, and the source distribution should be isotropic on the sky.

5.3. *The ROSAT XRT All-Sky Survey*

The position-sensitive proportional counter (PSPC) on board *ROSAT* has carried out an all-sky survey in the energy band 0.1–2.4 keV, with a sensitivity limit of 1.5×10^{-13} ECF^{-1} ergs s^{-1} cm^{-2}. The "energy-to-counts conversion factor" ECF takes into account the spectral response of the detector and interstellar absorption. Assuming blackbody emission from the source, we have computed it by interpolating data presented in the technical appendix of the *ROSAT* call for proposals.

We immediately deduce from Table 2 that the sampling depth is now much greater than 100 pc, well beyond the local cavity. Lines of sight in the Galactic plane must therefore sample the average interstellar medium with $n \simeq 1$ cm^{-3}, and therefore line of sight 1 should be typical for low latitudes. Source counts and maximum sampling depths for this as well as line of sight 4 toward a Galactic pole are presented in Table 3 and Figure 7. In contrast to the *EUVE* and WFC counts discussed above, polar cap accretion produces more sources because of the harder observing band (cf. eq. [30] above).

Comparing lines of sight 1 and 4 also shows that the sources will be very strongly concentrated toward the Galactic plane for both polar cap and isotropic accretion. This differs from the predictions of TC, who argued that a Galactic plane anisotropy would be visible only in longer exposures, deeper than the PSPC survey. This difference probably arises because they treated the interstellar medium as homogeneous, and so Galactic anisotropy could only be produced by the finite scale height of the NSs. As we discussed above in § 2.3, the interstellar scale height is much smaller and therefore has a much larger effect. As shown in Figure 4, our speed distributions also differ. While that of TC has many more low-velocity NSs, they have *no* NSs with speeds less than 25 km s^{-1}. Our small tail which extends to lower speeds will have higher accretion luminosities and give us larger sampling depths, thereby making it easier to see the anisotropy imposed by the Galaxy.

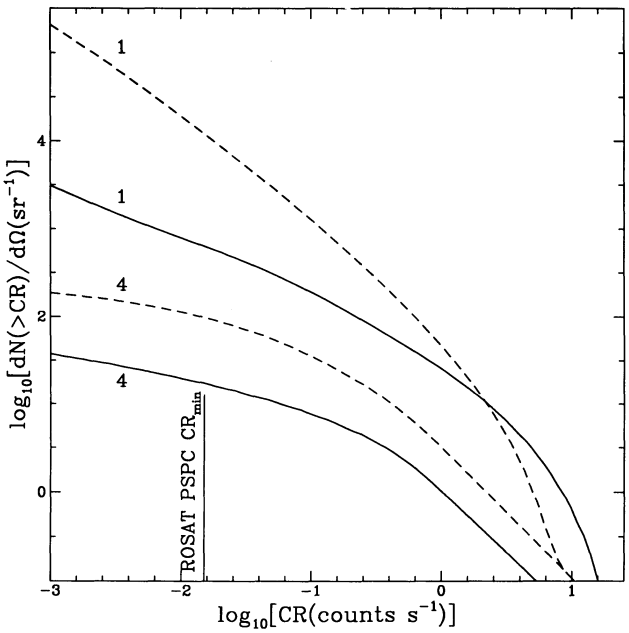

FIG. 7.—Cumulative source counts in the 0.1–2.4 keV band for the *ROSAT* PSPC and two lines of sight discussed in the text. Line of sight 1 has neutral material with density 0.07 cm^{-3} inside 100 pc and 1 cm^{-3} beyond, whereas line of sight 4 is the same but with no material beyond 100 pc. Solid curves are for isotropic accretion, and dashed curves are for polar cap accretion with $A_1 = 1$. The total number of Galactic neutron stars is taken to be 10^9.

The sampling depths in Table 3 indicate that most of the sources will be concentrated in $\simeq 3$ sr of sky for isotropic accretion and $\simeq 0.8$ sr of sky for polar cap accretion. Hence the total numbers of accreting NSs detectable by the all-sky survey are

$$N_{\rm PSPC}^{\rm iso} \simeq 2000\left(\frac{N_{\rm tot}}{10^9}\right) \quad (39)$$

and

$$N_{\rm PSPC}^{\rm cap} \simeq 10{,}000\left(\frac{N_{\rm tot}}{10^9}\right). \quad (40)$$

The PSPC survey could also detect NSs accreting material in nearby giant molecular clouds (GMCs) (cf. Table 1). The energy-to-counts conversion factor is ~ 0.15 for heavily absorbed ($N_{\rm H\,I} = 10^{22}$ cm^{-2}; cf. eq. [19]) blackbody spectra at $T_{\rm BB} \gtrsim 300$ eV. This yields a typical sensitivity of $\sim 10^{-12}$ ergs s^{-1} cm^{-2}. We will consider (see Table 2) the best case of polar cap accretion, since at lower temperatures the ECF drops to very low values. The scale height of molecular clouds is $H \sim 100$ pc (Scoville & Sanders 1987), and their volume filling factor can be estimated from Table 1 to be ff $\sim$ ff$_{-2.7} \times 10^{-2.7}$. The integrated source counts are given by

$$N(>S) = \Omega n_{\rm NS}\,{\rm ff}\left[\frac{S^{-3/2}}{24\pi^{3/2}}\int_0^{L_H} L^{3/2}p(L)dL + \frac{H}{8\pi S}\int_{L_H}^{\infty} Lp(L)dL - \frac{H^3}{6}\int_{L_H}^{\infty} p(L)dL\right], \quad (41)$$

where $p(L)$ is the luminosity function appropriate for GMC ambient densities ($n \sim 100$ cm^{-3}), $L_H = 4\pi H^2 S \sim 10^{30}$ ergs

© American Astronomical Society • Provided by the NASA Astrophysics Data System

1993ApJ...403..690B

s^{-1}, and we have assumed a constant NS space density. For the given parameters, the term on the right-hand side proportional to S^{-1} dominates the counts. We estimate

$$N^{\rm cap}_{\rm PSPC\text{-}GMC} \sim 1000 {\rm ff}_{-2.7} \left(\frac{N_{\rm tot}}{10^9}\right) \quad (42)$$

and a sampling depth of ~ 5 kpc. These additional sources will therefore be tightly concentrated toward the Galactic plane.

5.4. *Constraints from the Einstein Extended Medium-Sensitivity Survey*

The *Einstein* Extended Medium-Sensitivity Survey (EMSS) of serendipitous sources (Gioia et al. 1990) was performed in the band 0.3–3.5 keV, and covered 778 $\deg^2$ at high latitude with a limiting sensitivity of 3.36×10^{-12} ergs s^{-1} cm^{-2} (smaller areas were covered with a much greater sensitivity). All sources above this threshold have been (optically) identified (Gioia et al. 1990). Neglecting absorption because of the hard observing band, equation (33) along line of sight 4 yields a lower limit to the expected number of observable NSs,

$$N^{\rm cap}_{\rm EMSS} \simeq 1600 \left(\frac{n_{\rm NS}}{\rm pc^{-3}}\right), \quad (43)$$

which is consistent with the lack of unidentified sources (as candidate isolated NSs) for $n_{\rm NS} \lesssim 6 \times 10^{-4}$ pc^{-3}. This number is in agreement with the estimated NS number density in equation (13) for $N_{\rm tot} \lesssim 10^9$. For isotropic accretion, again, even the Oort limit is consistent with no observed NSs.

5.5. *Diffuse Galactic X-Ray Emission*

With a vertically integrated surface density of $0.7(N_{\rm tot}/10^9)$ pc^{-2} (cf. eq. [14]), isolated NSs accreting material in the Galactic plane might represent a substantial population of low-luminosity X-ray sources, and their cumulative effects have observable consequences. In an ambient medium with $n \simeq 1$ cm^{-3}, the average NS luminosity in the 2–6 keV band is $\langle L^{\rm cap} \rangle = 1.2 \times 10^{29}$ ergs s^{-1}. In the solar region, isolated NSs could then contribute a volume emissivity

$$\epsilon^{\rm cap}(2\text{–}6 \text{ keV}) \simeq 1.2 \times 10^{26} \left(\frac{n_{\rm NS}}{10^{-3} \text{ pc}^{-3}}\right) \text{ergs s}^{-1} \text{ pc}^{-3}, \quad (44)$$

with $\epsilon^{\rm iso}(2\text{–}6$ keV) being many orders of magnitude smaller. These estimates assume a Planckian spectrum. Note that, since we are in the Wien regime, the X-ray emissivity is also fairly sensitive to the background density. Increasing n by a factor of 3 increases $\epsilon^{\rm cap}(2\text{–}6$ keV) by almost a factor of 10. The contribution in the 2–6 keV band could be larger if a substantial fraction of the NS bolometric luminosity is not thermalized and emerges at X-ray energies.

5.5.1. *The Soft X-Ray Background*

Ostriker et al. (1970) have suggested that the soft X-ray background (SXRB) might arise from the superposition of discrete sources such as accreting NSs, rather than being truly diffuse. The measured SXRB intensity at 100 eV is $\sim 3 \times 10^{-23}$ ergs s^{-1} cm^{-2} Hz^{-1} (McCammon et al. 1983). In the best case of isotropic accretion, and assuming that line of sight 1 is typical of the local cavity, we find that the integrated NS flux detectable near the Sun is

$$S_\nu \simeq 3 \times 10^{-26} \left(\frac{n_{\rm NS}}{7.5 \times 10^{-4} \text{ pc}^{-3}}\right) \text{ergs s}^{-1} \text{ cm}^{-2} \text{ Hz}^{-1}. \quad (45)$$

It is clear that, unless the local NS density is much larger than estimated, and there exist many more slowly moving stars, local NSs will make a negligible, $\sim 0.1\%$, contribution to the SXRB (cf. Ostriker et al. 1970). With the derived speed distribution at equilibrium, the NS contribution to the SXRB would increase only up to 7% of the total if the local NS number density approached the Oort limit.

5.5.2. *The Galactic X-Ray Ridge Observed by EXOSAT*

A bright Galactic ridge component within $\pm 40°$ longitude of the Galactic center has been observed by *EXOSAT* in the 2–6 keV range (Warwick et al. 1985). The excess X-ray flux, which is not explained in terms of known discrete sources, has a scale height of ~ 100 pc and an X-ray luminosity of $\sim 10^{38}$ ergs s^{-1}. From a comparison with *Einstein* observations in the Galactic plane, Warwick et al. (1985) concluded that the bulk of the observed emission must arise, assuming a discrete source origin, in a low X-ray luminosity population, $L_x < 10^{33.5}$ ergs s^{-1}, with at least 3×10^4 sources contributing to the ridge. The *EXOSAT* ridge finds a natural explanation in terms of our population of isolated NSs accreting material in the Galactic plane.

Because of the high sensitivity of the NS luminosity in this energy range to the interstellar density, a detailed comparison with the surface brightness profile of the ridge requires a detailed model of the interstellar medium. We therefore limit ourselves here to a crude estimate. Interior to the ridge, $R < R_D \equiv R_0 \sin 40° \simeq 5.5$ kpc, the interstellar density is dominated by molecular material with typical volume-averaged density of ~ 5 cm^{-3} and scale height ~ 100 pc (Scoville & Sanders 1987). Assuming that the NS speed distribution is similar to that locally, the mean luminosity for polar cap accretion is $\langle L^{\rm cap}(2\text{–}6 \text{ keV}) \rangle \simeq 3 \times 10^{30}$ ergs s^{-1}. We take the equilibrium radial NS distribution to be similar to the probability density at birth given in equation (5), but renormalized to agree with equation (13) at $R = R_0$. We find that there are $\simeq 6 \times 10^7 (n_{\rm NS}/10^{-3}$ $pc^{-3})$ NSs in the region $R < R_D$ and $|z| < 100$ pc. Hence the contribution of unresolved accreting NS sources to the *EXOSAT* ridge is

$$L^{\rm cap}_{\rm ridge}(2\text{–}6 \text{ keV}) \sim 10^{38} \left[\frac{n_{\rm NS}(R_0)}{10^{-3} \text{ pc}^{-3}}\right] \text{ergs s}^{-1}, \quad (46)$$

consistent with the *EXOSAT* observations.

The NS scale height (see eq. [15]) is substantially larger than that of the cold atomic and molecular interstellar phases with $n \gtrsim 1$ cm^{-3}. However, it is comparable to or smaller than the scale heights of the more extended warm neutral and warm ionized phases, which together have $n \sim 0.2$ cm^{-3} (Kulkarni & Heiles 1987; BR91). Hence we would expect a fainter, more extended source of diffuse X-ray emission with larger scale height than that of the *EXOSAT* ridge. Such emission, with a scale height $\simeq 250$ pc, has been detected at $|l| > 50°$ by *HEAO 1* A-2 (Worrall et al. 1982).

6. NEUTRON STARS ACCRETING IN DENSE INTERSTELLAR CLOUDS

6.1. *Cometary* H II *Regions*

The UV and X-ray emission from an accreting NS will ionize ambient atomic and molecular gas, producing a characteristic observational signature which may be used to distinguish NSs from other sources on the sky. From the speed distribution in Figure 4 we expect that the majority of local

© American Astronomical Society • Provided by the NASA Astrophysics Data System

1993ApJ...403..690B

NSs move at highly supersonic speeds relative to the gas and, in particular, will leave their own Strömgren spheres in less than one recombination time scale (cf. Alcock & Illarionov 1980). The Strömgren radius is

$$r_S \equiv \left[\frac{3S}{4\pi n^2(1+\chi)\alpha_B}\right]^{1/3}, \quad (47)$$

where S is the emission rate of ionizing photons from the NS, $\chi = 0.2$ is a small correction factor due to the presence of ionized helium, and $\alpha_B = 2.6 \times 10^{-13}$ cm^3 s^{-1} is the recombination coefficient to the excited states of hydrogen at 10^4 K. Assuming isotropic accretion and pure blackbody emission, we find $S \simeq 2.4 \times 10^{40} n^{3/4} v_{40}^{-9/4}$ photons s^{-1} for $v_{40} \lesssim n^{1/3}$. Thus

$$r_S \simeq 2.6 \times 10^{17} n^{-5/12} v_{40}^{-3/4} \text{ cm} . \quad (48)$$

In the case of an ionizing star in motion relative to a homogeneous medium, the Strömgren sphere is distorted into a "cometary" H II region. Assuming that the front remains sharp and in steady state, its distance r from the star satisfies the equation (Thuan 1975; Raga 1986)

$$\frac{1}{3}(r_S^3 - r^3)n(1+\chi)\alpha_B = r^2 v \frac{\cos\xi}{\cos(\theta - \xi)}, \quad (49)$$

where θ is the polar angle of a point on the front, with $\theta = 0$ being in the direction of motion of the star, and ξ is the angle between the stellar velocity and the outward normal of the front. Raga (1986) presents numerical solutions to equation (49), but we may obtain analytic estimates in the following way.

After some manipulation, equation (49) may be rewritten as

$$\frac{d\eta}{d\theta} = \frac{1 - \eta^3 - \beta\eta^2\cos\theta}{\beta\eta\sin\theta}, \quad (50)$$

where $\eta \equiv r(\theta)/r_S$, $\beta \equiv 3t_{rec}/t_c$, and $t_c \equiv r_S/v$ and $t_{rec} \equiv [n(1+\chi)\alpha_B]^{-1}$ are the crossing and recombination time scales, respectively. Not surprisingly, the ratio of these two time scales determines the distortion of the Strömgren sphere. Most NSs will have $\beta \gg 1$, i.e., $v_{40} \gg 0.06 n^{1/3}$. In this regime, equation (50) has the following solution valid near the star ($\eta \lesssim 1$):

$$\beta\eta^2 = \frac{2}{1+\cos\theta} \quad (51)$$

(cf. Rasiwala 1969). Hence upwind of the star the I-front is at a distance

$$r(0) \simeq \beta^{-1/2} r_S \simeq 2 \times 10^{16} n^{-1/8} v_{40}^{-13/8} \text{ cm} , \quad (52)$$

while the maximum full width of the ionized region is $4r(0)$. Note that, as $r(0) \gg r_B$, the moving star excites an H II region of size larger than the accretion radius even in the case of a high-density environment, implying that accretion can indeed occur at the hydrodynamic rate given by equation (21). For the same reason, the density gradient in the accretion flow close to the star can be neglected in our Strömgren-type analysis.

Downwind of the NS ($\theta = 180°$), a long tail of ionized gas is left which slowly recombines. Although there will not be a sharp I-front here, we may still estimate the size of the ionized region from equation (50) in the $\eta \gg 1$ limit. This yields

$$\frac{\eta\sin\theta}{\eta\cos\theta + \beta} = \text{constant} . \quad (53)$$

Hence the size of the tail is

$$r(180) \simeq \beta r_S = 3 v t_{rec} \simeq 4 \times 10^{19} v_{40}\, n^{-1} \text{ cm} . \quad (54)$$

Equations (51) and (53) imply that the H II region has a conical shape, with volume $V_{H\,II} \simeq 4\pi r(0)^2 r(180)/3 \simeq 4\pi r_S^3/3$, as expected. Because accretion determines S, there is a velocity dependence:

$$V_{H\,II} \simeq 3 \times 10^{-3} n^{-5/4} v_{40}^{-9/4} \text{ pc}^{-3} . \quad (55)$$

It is worth remarking that, with the given parameters, the mean free path for an ionizing photon is $1.6 \times 10^{17} n^{-1}$ cm at threshold, and most of the blackbody photons which are emitted at $\sim 30 n^{1/4} v_{40}^{-3/4}$ eV will have even longer absorption lengths. It is therefore not appropriate to adopt a sharp boundary approximation for the I-front even ahead of the star, and the transition from neutral to ionized gas will be much more gradual. For high-density environments with $n \gtrsim 10 v_{40}^{13/7}$, photons near threshold will still generate a fully ionized region whose morphology will be described by equation (49), with S now being the emission rate of UV photons close to the ionization threshold, $\sim 7 \times 10^{39} n^{1/4} v_{40}^{-3/4}$ photons s^{-1}. Harder photons which penetrate more deeply into the surrounding neutral gas will produce ionizations with fast electrons. These electrons will in turn produce secondary ionizations and excitations giving rise to emission lines from a more extended region.

If the NS is moving through a molecular cloud, then reprocessing of the stellar radiation into the infrared becomes important. Lepp & McCray (1983) have considered the problem for an X-ray source at rest in a molecular cloud and find that $\sim 10\%$ of the stellar luminosity is reradiated in infrared emission lines from vibration-rotation transitions of H_2. Moreover, UV resonance lines such as Lyα, as well as a small fraction of the hard stellar photons (Böhringer, Morfill, & Zimmermann 1987), are absorbed by dust grains and reradiated in the far-infrared continuum. The effects of the NS's motion on the infrared reradiation need to be studied along the lines of our analysis above, but this is beyond the scope of this paper.

To summarize, an accreting NS in a GMC will produce a very elongated H II region of transverse dimension $\sim 10^{16}$ cm, corresponding to an angular size $\sim 2''$ at a fiducial distance of 300 pc. This could be resolved by radio observations of the free-free continuum and recombination line emission, which are largely unaffected by interstellar dust. We expect the H II region to lack the bow shock appearance of ultracompact H II regions near moving O stars (e.g., Van Buren et al. 1990) or pulsar wind nebulae (e.g., Kulkarni & Hester 1988), because the accretion flow will block the NS wind. If the star is moving through a molecular cloud, infrared line and continuum emission should also be detectable.

6.2. *Transient Emission*

Accretion of matter onto NSs in close binary systems is known to lead to unstable nuclear burning and to X-ray bursts (see, e.g., Joss & Rappaport 1984). We discuss here the intriguing possibility that the exploding material might be accumulated by slow accretion onto isolated NSs located in GMCs. For a NS with an ordinary interior, radius $R = 8.29$ km, and mass $M = 1.24\ M_\odot$, explosive helium burning requires accretion rates larger than $\dot{M}_{crit}^{He} \simeq 10^{13.3}$ g s^{-1} (Zdunik et al. 1992), which is above likely values even in the molecular phase of the ISM. From Figure 5 we estimate that only $\lesssim 2\%$ of NSs moving through an $n = 100$ cm^{-3} medium will have $\dot{M} > \dot{M}_{crit}^{He}$ ($v < 12$ km s^{-1}). Hydrogen burning is unstable for $\dot{M} > \dot{M}_{crit}^{H} \simeq 10^{13}$ g s^{-1} when the accreted gas has solar abundances, $\dot{M}_{crit}^{H}$ increasing with decreasing metallicity. At still

© American Astronomical Society • Provided by the NASA Astrophysics Data System

1993ApJ...403..690B

higher rates, $\dot{M} > 5\dot{M}^{\rm H}_{\rm crit}$ hydrogen burning is stabilized again because of the saturation effect of beta decays in the CNO cycle, leading to an energy generation rate which is totally insensitive to the temperature. Hameury, Heyvaerts, & Bonazzola (1983) have argued that, at very low accretion rates, sedimentation may reduce metallicity by 2–3 orders of magnitude. Recently, Bildsten, Salpeter, & Wasserman (1992) have found that, under some conditions, CNO nuclei may be destroyed at the stellar surface by spallation with free-falling protons, thereby further reducing the metallicity in the accreted envelope. We will simplify the complexity of theoretical shell flashes on accreting NSs by considering helium burning as the only way of triggering X-ray bursts. Below $\sim 10^{13}$ g s^{-1}, the hydrogen and helium shells near the surface are thermally stable, as burning proceeds in the pycnonuclear regime (Blaes et al. 1990).

6.2.1. *Isotropic Accretion*

The density at which helium is ignited is the highest (and the strongest bursts are expected) for accretion rates just above $\dot{M}^{\rm He}_{\rm crit}$, which corresponds to a critical $\Delta M_{\rm acc} \simeq 10^{-8.2}\ M_\odot$ of accumulated baryonic mass.[5] From Table 1 we estimate that, within 1 kpc, only ~ 20 objects will be able to accrete at $\dot{M} \gtrsim \dot{M}^{\rm He}_{\rm crit}$. Since the time interval between the shell flashes is $\Delta M_{\rm acc}/\dot{M}^{\rm He}_{\rm crit} \simeq 2 \times 10^4$ yr, the expected event rate is too small to be of observational interest.

6.2.2. *Accretion onto the Polar Cap*

The estimates above are substantially altered in the case of a magnetized object, since the flow is funneled onto the magnetic polar cap, and the local accretion rate per unit area is enhanced by a factor $f^{-1} \sim 10^3$ (Woosley & Wallace 1982). A larger fraction of the NS population might then undergo nuclear flashes, because rates above $\dot{M}^{\rm He}_{\rm crit} \simeq 10^{10.36}$ g s^{-1} km^{-2} could be reached even in a lower density environment. In the following, we will focus our attention on the $\sim 10\%$ of NSs which move at $v \lesssim 28$ km s^{-1}, and accrete $\gtrsim 2.8 \times 10^{12}$ g s^{-1} from a medium with $n = 100$ cm^{-3}. The effective rate is then $\dot{M} \gtrsim 2.8 \times 10^{12} A_1^{-1}$ g s^{-1} km^{-2} $\simeq 125\dot{M}^{\rm He}_{\rm crit}$. This is the inflow rate which characterizes "model B," the low-metallicity ($Z = 9 \times 10^{-4}$) model of Wallace, Woosley, & Weaver (1982). We will therefore extract the relevant properties of both the preexplosive evolution and thermonuclear outburst from this work. (Note that these authors consider a NS with radius $R = 14.3$ km and mass $M = 1.41\ M_\odot$.)

Since helium has a smaller mean molecular weight per electron than the (presumed) iron crust, a mountain forms above the NS surface if the accreted material is magnetically focused. The entire helium column is ignited in about 10 ms when $\Delta M_{\rm acc} \sim 5.5 \times 10^{19}$ g km^{-2}, depositing, as it burns to iron-peak elements, $\Delta E_{\rm He} \simeq 5 \times 10^{37}$ ergs km^{-2} of thermonuclear energy. It will take ~ 500 s to radiate all this energy at the Eddington flux, $F_{\rm E} = cGM/(\kappa_{\rm T} R^2) \simeq 10^{35}$ ergs s^{-1} km^{-2}, with a characteristic blackbody temperature $T_{\rm E} \simeq 2$ keV. By analogy with strong X-ray bursts (Tawara et al. 1984), a major expansion of the NS photosphere will occur as a consequence of the reduction of the Thomson scattering opacity $\kappa_{\rm T}$ in the burning, hot $T > 10^9$ K zone. All the super-Eddington energy flux which results is used to push the cooler, outer layers out, since the opacity there remains close to Thomson (Paczyński 1983). As argued by Woosley & Wallace (1982), the expanding plasma might cause the magnetic field to become highly distorted and prone to magnetic instabilities. A small fraction of the explosion energy, stored in the field, could be transferred to relativistic particles and produce γ-ray bursts.

It is also possible that a supersonic radiation-driven wind, free to expand laterally at large radii, might develop with terminal outflow velocity of $\sim 0.02c$ (Paczyński & Prószyński 1986). Only a small fraction, at most 1%, of the ashes of the outburst could be ejected from the deep gravitational well, as $\Delta M_{\rm out} < \Delta E_{\rm He} R/(GM)$ from energy considerations. The effects of this scaled-down version of a supernova blast on the surrounding medium are worth considering, as further accretion may be momentarily inhibited (see also Lasota 1992). The free-expansion phase of the outward-moving shock terminates at a distance

$$r_f \simeq 7 \times 10^{12} \left(\frac{\Delta M_{17.4}}{n_{100}}\right)^{1/3} \text{cm}\ , \tag{56}$$

which will be reached about 3 hr after the initial burst. Here $\Delta M_{17.4}$ is the injected mass in units of $10^{17.4}$ g, and n_{100} is the ambient density in units of 100 cm^{-3}. In the subsequent Sedov-Taylor phase, the shock radius evolves as

$$r_s \simeq 2.4 \times 10^{14} \left(\frac{\Delta E_{35}}{n_{100}}\right)^{1/5} t_y^{2/5} \text{ cm}\ , \tag{57}$$

slowing down according to

$$v_s \simeq 30 \left(\frac{\Delta E_{35}}{n_{100}}\right)^{1/5} t_y^{-3/5} \text{ km s}^{-1}\ , \tag{58}$$

where ΔE_{35} is the injected (kinetic) energy in units of 10^{35} ergs, and t_y is the elapsed time measured in years. The shocked gas will cool from a temperature

$$T_s \simeq 1.4 \times 10^4 \left(\frac{\Delta E_{35}}{n_{100}}\right)^{2/5} t_y^{-6/5} \text{ K} \tag{59}$$

in a time scale which is much longer than the dynamical time scales of interest. As the ejected material expands well beyond the accretion radius r_A in just a few hours, the accretion of interstellar gas will be effectively quenched, although only for ~ 5 yr. This is the time scale it will take a NS to move out of the region, through a distance $\sim 5 \times 10^{14}$ cm, and should be compared with the time interval between flashes in the absence of mass loss, $t_r = \Delta M_{\rm acc}/\dot{M} \simeq 0.6$ yr. The average residence time in a GMC is

$$t_c \simeq \frac{4R_{\rm cl}}{3v} \simeq 5.4 \times 10^5 \left(\frac{R_{\rm cl}}{30 \text{ pc}}\right)\left(\frac{v}{72 \text{ km s}^{-1}}\right)^{-1} \text{ yr}\ . \tag{60}$$

Each star could therefore produce $\sim 10^5$ helium flashes before leaving the high-density region. (Since helium burning releases ~ 100 times less energy per unit mass than the accretion process itself, transient phenomena make a negligible contribution to the global energy budget.) The expected rate of $\sim 5 \times 10^{37}$ erg events within ~ 1 kpc is then of order 25 yr^{-1}. Note that NSs moving faster with respect to the ambient medium (say $v \sim 50$ km s^{-1}) will accrete more slowly and produce bursts of larger energies ($\Delta E_{\rm He} \sim 8 \times 10^{38}$ ergs) at a much smaller rate (~ 1 yr^{-1}). It is clear that, in the γ-ray burst scenario put forward by Woosley & Wallace (1982), only a small fraction, $\sim 3\%$, of the 800 bursts per year detected by

[5] For $\dot{M} \simeq 10\dot{M}^{\rm He}_{\rm crit}$, $\Delta M_{\rm acc}$ decreases only by a factor ~ 2.5, then drops more rapidly at higher accretion rates (Zdunik et al. 1992). A rate $\dot{M} \gg \dot{M}^{\rm He}_{\rm crit}$ leads to a thinner helium layer and therefore produces a burst of smaller energy and shorter duration.

© American Astronomical Society • Provided by the NASA Astrophysics Data System

1993ApJ...403..690B

BATSE (Meegan et al. 1992) could be attributed to a thermonuclear flash mechanism. This small subset of events would obviously be characterized by strong anisotropies on the sky. For example, from Table 1 we predict a large concentration of events in the Cygnus region. It would be of interest to check whether any observed bursts could be positionally associated with nearby GMCs.

With a characteristic GMC absorbing column of (5–10) $\times 10^{21}$ cm^{-2}, the optical depth for photoelectric absorption (Morrison & McCammon 1983) is unity at a photon energy of 1–1.5 keV. X-ray bursts from NSs accreting in GMCs could then be detected by the *High Energy Transient Explorer* (*HETE*), which has an X-ray observing band of 2–10 keV and a sensitivity $\sim 8 \times 10^{-9}$ ergs cm^{-2} s^{-1} (Ricker et al. 1992). Such bursts may also be responsible for some of the observed fast X-ray transients (cf. Joss & Rappaport 1984). It is interesting to note that the *HEAO 1* A-1 transient H0422+27 (Ambruster & Wood 1986) is located in the direction of the Taurus GMC.

7. CONCLUSIONS

Our most important and interesting results are the estimated numbers of observable NSs presented in § 5. In particular, we predict that somewhere between tens and hundreds of NSs will be seen in the *EUVE* and *ROSAT* WFC surveys (eqs. [35]–[38] above). The *ROSAT* PSPC survey will see many more: between one and ten thousand (eqs. [39] and [40] above) sources accreting from the local interstellar medium and possibly a further 1000 from nearby molecular clouds (eq. [42]). Moreover, accreting NSs can make a significant contribution to the global diffuse X-ray emission from the Galaxy, although their contribution to the soft X-ray background is minimal. These estimates depend on a number of important uncertainties:

1. Assuming that the kinematic properties of the observed population of radio pulsars are representative of young NSs, we were able in § 2 above to calculate the local space and speed distributions of old NSs. Even if this assumption is correct, however, the radio pulsar birth distributions, particularly at the very important low peculiar velocities, must still be considered somewhat uncertain. (So is the overall Galactic gravitational potential, but we believe this to be much less important.) The thin-disk approximation can be used to explore the parameter space, and new estimates can quickly be made should better distributions become available.

2. The local NS space density also depends on the total number $N_{\rm tot}$ of NSs produced throughout the history of the Galaxy. As we mentioned in § 2.3 above, this number is only known to within a factor of 10. Observing old NSs will of course help to pin this number down better.

3. In § 3 we summarized what is generally known about the geography of the local interstellar medium. The ambient particle density determines both the accretion rate and the severity of absorption. The most important uncertainties here are the pervasiveness of the coronal gas responsible for the soft X-ray background and the amount of denser ionized material.

4. As we discussed in § 4.1, we cannot be sure what fraction of NSs can accrete from the interstellar medium until the propeller mechanism and magnetic field evolution and topology are better understood.

5. The luminosity produced by an accreting NS in the various observing bands depends on the emission spectrum. In all our numerical estimates in § 5 we have taken the most conservative, naive approach and assumed a blackbody spectrum. As we discussed in § 4.3, this is very uncertain, and there are good reasons to believe that the production of photons in the higher energy observing bands is much more efficient. This will increase the numbers of detectable sources, which if observed will provide a handle on the accretion physics.

Our treatment of points 1 and 4 assumed that all old NSs passed through an isolated radio pulsar phase similar to those we observe today. It is important to bear in mind that up to now the only way of detecting isolated NSs relied on their being magnetized and spinning rapidly. Because of the barriers to accretion that this produces, as well as the observed correlation between magnetic field and peculiar velocity (cf. eq. [12] above), NSs which do *not* pass through a radio pulsar phase are likely to be stronger accretors. Bhattacharya & van den Heuvel (1991) have made the interesting suggestion that possibly as many as several tens of percents of isolated NSs may have formed from Thorne-Żytkow objects produced in a common-envelope spiraling-in of the NSs in tight massive X-ray binaries. These NSs will have low space velocities relative to the interstellar medium and possibly weak magnetic fields. Provided they are not spinning too rapidly, such NSs could accrete material at very high rates.

It is important to be able to distinguish accreting NSs from other EUV and X-ray sources. The simplest (and most revealing) diagnostics are that NSs are faint and hot, and lack optical counterparts: a nonmagnetized source in the local cavity will have a typical surface temperature $\sim 100{,}000$ K and a B-magnitude ~ 27.6 at 100 pc. In addition, accreting NSs will be correlated with the denser phases of the interstellar medium. In particular, we expect a substantial source concentration toward the Galactic plane in all surveys except for both *EUVE* and *ROSAT* WFC in the case of polar cap accretion. Further observation should reveal some additional characteristic signatures. If accretion is concentrated onto polar caps, then rotation of the star may cause the emission to be pulsed. Because of the expected long periods (cf. eq. [27]), only long integrations will be able to reveal a periodicity. As suggested by TC, high proper motions should exist in some sources, although we predict an inverse correlation between this and observed flux. Radio detection of cometary H II regions around the NSs should be feasible, and the NSs will also have associated infrared emission (§ 6.1). Accreting NSs may make a significant contribution to "diffuse" X-ray emission features in the Galaxy (§ 5.5), in particular the ridge observed by *EXOSAT*. They may also be detectable as sources of transient X-ray emission (§ 6.2).

In addition to the exciting possibility of detecting a completely new class of astronomical sources, observations of accreting isolated NSs will provide an important handle on NS evolution over Gyr time scales. Currently such ages are observable only for NSs in binaries, where it is clear that the star's membership in the binary has had a strong effect on its evolution. Important questions such as how the magnetic field evolution over Gyr time scales. Currently such ages are observable only for NSs in binaries, where it is clear that the star's

It is a pleasure to thank L. Bildsten, L. Binette, G. De Marchi, A. Meiksin, M. Merrifield, R. Nelson, B. Paczyński, N. Panagia, S. Tremaine, and J. Wang for informative discussions and comments. P. M. thanks the organizers of the Aspen Center for Physics' Astrophysics Workshop for their hospitality. O. B. is supported by the Canadian NSERC.

© American Astronomical Society • Provided by the NASA Astrophysics Data System

1993ApJ...403..690B

REFERENCES

Alcock, C., & Illarionov, A. 1980, ApJ, 235, 541
Ambruster, C. W., & Wood, K. S. 1986, ApJ, 311, 258
Arnett, W. D., Schramm, D. N., & Truran, J. W. 1989, ApJ, 339, L25
Arons, J., & Lea, S. M. 1980, ApJ, 235, 1016
Bhatt, H. C. 1990, A&A, 232, 367
Bhattacharya, D., & van den Heuvel, E. P. J. 1991, Phys. Rep., 203, 1
Bhattacharya, D., Wijers, R. A. M. J., Hartman, J. W., & Verbunt, F. 1992, A&A, 254, 198
Bildsten, L., Salpeter, E. E., & Wasserman, I. 1992, ApJ, 384, 143
Binney, J., & Tremaine, S. 1987, Galactic Dynamics (Princeton: Princeton Univ. Press)
Blaes, O., Blandford, R. D., Madau, P., & Koonin, S. 1990, ApJ, 363, 612
Blaes, O., Blandford, R. D., Madau, P., & Yan, L. 1992, ApJ, 399, 634
Blaes, O., & Rajagopal, M. 1991, ApJ, 381, 210 (BR91)
Bochkarev, N. G. 1987, Ap&SS, 138, 229
Böhringer, H., Morfill, G. E., & Zimmermann, H. U. 1987, ApJ, 313, 218
Bowyer, S., Jelinsky, P., Christian, C., & Malina, R. F. 1992, in Proc. Seventh Cambridge Workshop, Cool Stars, Stellar Systems, and the Sun, ed. M. S. Giampapa & J. A. Bookbinder (San Francisco: ASP), 613
Bruhweiler, F. C., & Vidal-Madjar, A. 1987, in Exploring the Universe with the *IUE* Satellite, ed. Y. Kondo (Dordrecht: Reidel), 467
Cox, D. P., & Reynolds, R. J. 1987, ARA&A, 25, 303
Dame, T. M., et al. 1987, ApJ, 322, 706
Davidson, K., & Ostriker, J. P. 1973, ApJ, 179, 585
Davies, R. E., Fabian, A. C., & Pringle, J. E. 1979, MNRAS, 186, 779
Davies, R. E., & Pringle, J. E. 1981, MNRAS, 196, 209
Frei, Z., Huang, X., & Paczyński, B. 1992, ApJ, 384, 105 (FHP)
Frisch, P. C., & York, D. G. 1991, in Extreme Ultraviolet Astronomy, ed. R. F. Malina & S. Bowyer (New York: Pergamon), 322
Gioia, I. M., Maccacaro, T., Schild, R. E., Wolter, A., Stocke, J. T., Morris, S. L., & Henry, J. P. 1990, ApJS, 72, 567
Gry, C., York, D. G., & Vidal-Madjar, A. 1985, ApJ, 296, 593
Hameury, J. M., Heyvaerts, J., & Bonazzola, S. 1983, A&A, 121, 259
Harding, A. K., & Leventhal, M. 1992, Nature, 357, 388
Hartmann, D., Epstein, R. I., & Woosley, S. E. 1990, ApJ, 348, 625
Helfand, D. J., Chanan, G. A., & Novick, R. 1980, Nature, 283, 337
Hunt, R. 1971, MNRAS, 154, 141
Illarionov, A., & Sunyaev, R. 1975, A&A, 39, 185
Iwan, D. 1980, ApJ, 239, 316
Joss, P. C., & Rappaport, S. A. 1984, ARA&A, 22, 537
Juda, M., Bloch, J. J., Edwards, B. C., McCammon, D., Sanders, W. T., Snowden, S. L., & Zhang, J. 1991, ApJ, 367, 182
Kulkarni, S. R. 1986, ApJ, 306, L85
Kulkarni, S. R., & Heiles, C. 1987, in Ap&SS Library, Vol. 134, Interstellar Processes, ed. D. J. Hollenbach & H. A. Thronson, Jr. (Dordrecht: Reidel), 87
Kulkarni, S. R., & Hester, J. J. 1988, Nature, 335, 801
Langer, S. H., & Rappaport, S. 1982, ApJ, 257, 733
Lasota, J.-P. 1992, in Gamma-Ray Bursts, ed. C. Ho, R. I. Epstein, & E. E. Fenimore (Cambridge: Cambridge Univ. Press), 17
Lepp, S., & McCray, R. 1983, ApJ, 269, 560
Lyne, A. G., Manchester, R. N., & Taylor, J. H. 1985, MNRAS, 213, 613
McCammon, D., Burrows, D. N., Sanders, W. T., & Kraushaar, W. L. 1983, ApJ, 269, 107
Meegan, C. A., Fishman, G. J., Wilson, R. B., Paciesas, W. S., Pendleton, G. N., Horack, J. M., Brock, M. N., & Kouveliotou, C. 1992, Nature, 355, 143
Morrison, R., & McCammon, D. 1983, ApJ, 270, 119
Myers, P. C., & Goodman, A. A. 1988, ApJ, 329, 392
Narayan, R., & Ostriker, J. P. 1990, ApJ, 352, 222 (NO)
Nelson, R. W., Salpeter, E. E., & Wasserman, I. 1992, in Proc. Workshop on the Physics of Isolated Pulsars (Taos), in press
Nomoto, K., & Tsuruta, S. 1987, ApJ, 312, 711
Ostriker, J. P., Rees, M. J., & Silk, J. 1970, Astrophys. Lett., 6, 179
Paczyński, B. 1983, ApJ, 267, 315
———. 1990, ApJ, 348, 485
Paczyński, B., & Prószyński, M. 1986, ApJ, 302, 519
Paresce, F. 1984, AJ, 89, 1022
Pounds, K. A., et al. 1991, MNRAS, 253, 364
Raga, A. C. 1986, ApJ, 300, 745
Rasiwala, M. 1969, A&A, 1, 431
Ricker, G. R., et al. 1992, in Gamma-Ray Bursts, ed. C. Ho, R. I. Epstein, & E. E. Fenimore (Cambridge: Cambridge Univ. Press), 288
Scoville, N. Z., & Sanders, D. B. 1987, in Ap&SS Library, Vol. 134, Interstellar Processes, ed. D. J. Hollenbach & H. A. Thronson, Jr. (Dordrecht: Reidel), 21
Shapiro, S. L., & Salpeter, E. E. 1975, ApJ, 198, 671
Snowden, S. L., Cox., D. P., McCammon, D., & Sanders, W. T. 1990, ApJ, 354, 211
Tawara, Y., et al. 1984, ApJ, 276, L41
Thuan, T. X. 1975, ApJ, 198, 307
Treves, A., & Colpi, M. 1991, A&A, 241, 107 (TC)
Turner, B. E. 1988, in Galactic and Extragalactic Radio Astronomy, ed. G. L. Verschuur & K. I. Kellermann (New York: Springer), 154
Ungerechts, H., & Thaddeus, P. 1987, ApJS, 63, 645
Van Buren, D., Mac Low, M.-M., Wood, D. O. S., & Churchwell, E. 1990, ApJ, 353, 570
Vanderhill, M. J., Borken, R. J., Bunner, A. N., Burstein, P. H., & Kraushaar, W. L. 1975, ApJ, 197, L19
Wallace, R. K., Woosley, S. E., & Weaver, T. A. 1982, ApJ, 258, 696
Wang, Y.-M., & Robertson, J. A. 1985, A&A, 151, 361
Warwick, R. S., Turner, M. J. L., Watson, M. G., & Willingale, R. 1985, Nature, 317, 218
Woosley, S. E., & Wallace, R. K. 1982, ApJ, 258, 716
Worrall, D. M., Marshall, F. E., Boldt, E. A., & Swank, J. H. 1982, ApJ, 255, 111
Zdunik, J. L., Haensel, P., Paczyński, B., & Miralda-Escudé, J. 1992, ApJ, 384, 129
Zel'dovich, Ya. B., & Shakura, N. I. 1969, Soviet Astron.—AJ, 13, 175

© American Astronomical Society • Provided by the NASA Astrophysics Data System